

An-Najah National University

Faculty of Graduate Studies

**Noncovalent Functionalization of Carbon
Nanomaterials as a Scaffold for Tissue Engineering**

By

Sahar Eyad Alhaj Qasem

Supervisors

Dr. Mohyeddin Assali

Dr. Naim Kittana

**This Thesis is Submitted in Partial Fulfillment of the Requirements for
the Degree of Master in Pharmaceutical Sciences, Faculty of Graduate
Studies, An-Najah National University, Nablus, Palestine.**

2020

**Noncovalent Functionalization of Carbon
Nanomaterials as a Scaffold for Tissue Engineering**

By

Sahar Eyad Alhaj Qasem

This Thesis was Defended Successfully on 30/8/2020 and approved by:

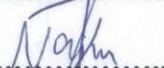
Defense Committee Members

Signature

1. Dr. Mohyeddin Assali / Supervisor

.....

2. Dr. Naim Kittana / Co-Supervisor

.....

3. Dr. Hussein Hallak / External Examiner

.....

4. Dr. Ramzi Shawahna / Internal Examiner

.....

Dedication

This is dedicated to:

The greatest dad and mum in the whole world for their unconditional love, prayers, endless support and making me realize that I am worth everything in this life. I am glad to call you my parents.

My beloved brothers and sisters for being the pillows and cheerleading squad I have needed. I love you endlessly.

A very special little one, my nephew, Adam who fills my life with laughter and happiness. I love you to the moon and back.

All the people in my life who touch my soul somehow.

Acknowledgment

At first, I thank Allah for giving me the courage and the determination, as well as guidance to achieve this research, despite all difficulties. I am truly grateful for your exceptional love and grace during this entire life.

I also extend my heartfelt gratitude to my supervisor, Dr. Mohyeddin Assali. You were such a great motivator even when the ride seemed tough for me. Thanks for your valuable advice. And deepest thanks to Dr. Naim Kittana for his scientific support and constructive advice.

I would like to thank the rest of the examination committee, for reading my thesis, their insightful comments and suggestions and invaluable criticisms.

Thanks to Dr. Muna Hajj Yahya, Department of Physics, Faculty of Science, at An-Najah National University for her collaboration in conductivity measurements.

Thanks to An-Najah University Hospital for its collaboration in the histopathological evaluation.

Thanks to Cell Therapy Center (CTC) at the University of Jordan for their collaboration in SEM measurements.

Thanks to Hamdi Mango Center for Scientific Research, Faculty of Medicine and Faculty of Science at the University of Jordan for their collaboration in NMR, TEM and TGA measurements.

I'm thankful to the staff of the laboratories of the College of Pharmacy, Science and Medicine for supplying help and assistance. Especially, the supervisor of the laboratories of the College of Pharmacy Mr. Mohammad Arar and the lab workers Tahreer Shtayeh, Linda Arar and Sundus Hilali and mostly the supervisor of laboratories of the College of Medicine Mr. Ahmed Musa.

My colleagues in the Department of Pharmacy thank you for your help and all the sweet memories we created together.

However, most of all this work would not have been completed without the love, help and facilities provided by my precious family. I wish I could make you always proud.

Sahar Alhaj Qasem.

الإقرار

أنا الموقعة أدناه مقدمة الرسالة التي تحمل العنوان:

**Noncovalent functionalization of carbon nanomaterials as a scaffold
for tissue engineering**

أقر بأن ما اشتملت عليه الرسالة هو نتاج جهدي الخاص، باستثناء ما تمت الإشارة إليه حيثما ورد، وأن هذه الرسالة ككل، أو أي جزء منها لم يقدم من قبل لنيل أي درجة أو لقب علمي أو بحثي لدى أي مؤسسة تعليمية أو بحثية أخرى.

Declaration

The work provides in this thesis, unless otherwise referenced, is the researcher's own work, and has not been submitted elsewhere for any other degree or qualification.

Student's Name: Sahar Eyad Alhaj Gaseem

إسم الطالبة:

Signature: Sahar

التوقيع:

Date: 30 / 8 / 2020

التاريخ

Table of Contents

NO.	Subject	Page
	Dedication	Iii
	Acknowledgement	Iv
	Declaration	Vi
	List of Tables	X
	List of Figures	Xi
	List of Schemes	Xv
	List of Abbreviations	Xvi
	Abstract	Xviii
	Chapter One: Introduction	1
1.1	Carbon allotropes	1
1.1.1	Carbon nanotubes	2
1.1.2	Graphene	3
1.2	Functionalization of CNTs and graphene	4
1.2.1	Covalent functionalization	4
1.2.1.1	Covalent functionalization of CNTs	5
1.2.1.2	Covalent functionalization of graphene	6
1.2.2	Non-covalent functionalization	7
1.2.2.1	Non-covalent functionalization of CNTs	8
1.2.2.2	Non-covalent functionalization of graphene	9
1.3	Regenerative medicine	10
1.3.1	Regenerative pharmacology	11
1.3.2	Tissue engineering	12
1.4	Literature Review	16
1.5	Aims of the study	22
1.6	Objectives	22
1.7	The importance of this project	23
1.8	General approach of the synthesis and functionalization of CNTs and graphene	24
	Chapter Two: Methodology	28
2.1	Reagents and materials	28
2.2	Instrumentation	30
2.3	Synthesis and characterization of the products	31
2.3.1	Synthesis of OH-TEG-alkyne (1)	31
2.3.2	Synthesis of Pyrene-TEG-alkyne (2)	32
2.3.3	Synthesis of OH-TEG-Tosyl (3)	33
2.3.4	Synthesis of OH-TEG-N ₃ (4)	33
2.3.5	Synthesis of COOH-TEG-N ₃ (5)	33
2.3.6	Synthesis of Pyrene-TEG-triazole-TEG-OH (6)	34
2.3.7	Synthesis of Pyrene-TEG-triazole-TEG-COOH (7)	35

2.4	Optimization of the needed amount of compound (6) or (7) to functionalize SWCNTs, MWCNTs and graphene in H ₂ O	36
2.5	Connective tissues casting and characterization	36
2.5.1	Generation of engineered connective tissues (ECTs)	36
2.5.1.1	Normal DMEM growth medium preparation	36
2.5.1.2	2x DMEM preparation	37
2.5.1.3	Preparation of sterile 0.1 N NaOH for tissue generation	37
2.5.1.4	Stock solutions preparation	38
2.5.1.4.1	SWCNTs-OH, MWCNTs-OH, SWCNTs-COOH and MWCNTs-COOH	38
2.5.1.4.2	Graphene-OH and graphene-COOH	38
2.5.1.5	Cell suspension preparation	38
2.5.1.5.1	3T3 cells	38
2.5.1.5.2	Primary skin fibroblasts	39
2.5.1.6	Preparation of engineered connective tissues (ECTs)	40
2.5.2	Electrical conductivity of ECTs	41
2.5.3	Cell viability test	42
2.5.3.1	Cell culture	42
2.5.3.2	Stock solution preparation with serial dilutions	43
2.5.3.2.1	SWCNTs-OH, MWCNTs-OH, SWCNTs-COOH and MWCNTs-COOH	43
2.5.3.2.2	Graphene-OH and graphene-COOH	43
2.5.3.3	3-(4,5-dimethylthiazol-2-yl)-5-(3-carboxymethoxyphenyl)-2-(4-sulfophenyl)-2H-tetrazolium (MTS) assay	44
2.5.4	Histopathological evaluation for ECTs	44
2.5.5	SEM evaluation for ECTs	45
2.5.6	Statistical evaluation for ECTs	45
	Chapter Three: Results and Discussion	46
3.1	Synthesis and functionalization of carbon nanomaterials	46
3.1.1	Synthesis of Pyrene conjugates	46
3.1.2	Non-covalent functionalization of carbon nanostructures	48
3.2	Characterization of functionalized carbon nanomaterials	50
3.2.1	Dispersibility of the functionalized carbon nanomaterials	50
3.2.2	Size and morphology of carbon nanomaterials	51
3.2.3	UV-vis spectrophotometry	52
3.2.4	Thermogravimetric analysis (TGA)	53
3.2.5	Zeta potential	54
3.3	Connective tissues casting and characterization	55
3.3.1	3T3 cells-based ECTs	55

3.3.1.1	Generation of ECTs with 3T3 cells	55
3.3.1.2	Electrical conductivity of ECTs	56
3.3.1.3	Cell viability test	58
3.3.1.4	Histopathological evaluation for ECTs	60
3.3.1.5	SEM evaluation for ECTs	64
3.3.1.5.1	Analysis of Fiber thickness	66
3.3.1.5.2	Analysis of Matrix porosity	66
3.3.2	Primary skin fibroblasts-based ECTs	68
3.3.2.1	Generation of ECTs with Primary skin fibroblast	68
3.3.2.2	Electrical conductivity of ECTs	70
3.3.2.3	Histopathological evaluation for ECTs	71
3.3.2.4	SEM evaluation for ECTs	74
3.3.2.4.1	Analysis of Fiber thickness	75
3.3.2.4.2	Analysis of Matrix porosity	75
	Conclusion	77
	References	79
	الملخص	ب

List of Tables

NO.	Table Title	Page
1	The general composition of ECT.	41
2	Zeta potential values for all of our functionalized carbon nanostructures.	55

List of Figures

NO.	Figure title	Page
1.1	Some carbon allotropes.	1
1.2	A) SWCNTs; B) MWCNTs.	2
1.3	Graphene structure.	3
1.4	Covalent functionalization of CNTs.	6
1.5	Covalent functionalization of graphene.	7
1.6	Noncovalent adsorption of single-walled carbon nanotube with 1-pyrenebutanoic acid, succinimidyl ester via π - π stacking.	8
1.7	Schematic representation of the synthesis of the Tbf-linked carbohydrate-MWCNTs.	9
1.8	General scheme for regenerative pharmacology.	12
1.9	Tissue engineering approach for tissue regeneration.	13
1.10	Schematic of process by which CNT can be incorporated into collagen fibrils.	18
1.11	Schematic diagram of the construct preparation process.	19
1.12	Schematic illustration of the rGO-GelMA synthesis process.	21
1.13	Schematic representation to describe the study.	22
3.1	Image of dispersion of (A) p-SWCNTs, (B) SWCNTs-Py-OH and (C) SWCNTs-Py-COOH.	50
3.2	Image of dispersion of (A) p-MWCNTs, (B) MWCNTs-Py-OH and (C) MWCNTs-Py-COOH.	51
3.3	Image of dispersion of (A) p-graphene, (B) Graphene-Py-OH and (C) Graphene-Py-COOH.	51
3.4	TEM images of A) f-graphene; B) f-MWCNTs and C) f-SWCNTs.	52
3.5	UV-Vis spectra of A) Py-OH, Graphene-Py-OH, MWCNTs-Py-OH, SWCNTs-Py-OH and B) Py-COOH, Graphene-Py-COOH, MWCNTs-Py-COOH, SWCNTs-Py-COOH.	53
3.6	Thermogravimetric analysis of all functionalized carbon nanomaterials: A) Graphene-Py-COOH; B) Graphene-Py-OH; C) MWCNTs-Py-COOH; D) MWCNTs-Py-OH; E) SWCNTs-Py-COOH; F) SWCNTs-Py-OH.	54
3.7	Gross examination of 3T3-containing ECT with varying CNTs or graphene loading: A) Control; B) SWCNTs-Py-OH (0.050%); C) SWCNTs-Py-COOH (0.050%); D) MWCNTs-Py-OH (0.050%); E) MWCNTs-Py-COOH (0.050%); F) Graphene-Py-OH (0.010%) and G) Graphene-Py-COOH (0.010%).	56
3.8	Average electrical conductivity of ECT constructs of 3T3 cells with different A) CNTs loading or B) graphene loading. The symbol * indicates significance ($P \leq 0.05$) with respect to control (0.000%). The statistical significance was determined by two-way ANOVA.	57

3.9	Average electrical conductivity of ECT constructs of 3T3 cells with the highest A) CNTs loading or B) graphene loading. The symbol * indicates significance ($P \leq 0.05$) with respect to control. The statistical significance was determined by Student t-test.	58
3.10	Bright field images at 100× for 3T3 cells treated with different concentrations of CNTs (0.025%, 0.050% and 0.100%), images 1-3, respectively or graphene (0.005%, 0.010% and 0.020%), images 1-3, respectively after 48 hours : A) Control (3T3 cells without treatment); B) SWCNTs-Py-OH; C) SWCNTs-Py-COOH; D) MWCNTs-Py-OH; E) MWCNTs-Py-COOH; F) Graphene-Py-OH and G) Graphene-Py-COOH.	59
3.11	Concentration-dependent effect of A) CNTs species or B) graphene species on the viability of 3T3 cells over 24 hours. The symbol * indicates significance ($P \leq 0.05$) with respect to control (0.000%). The statistical significance was determined by two-way ANOVA.	60
3.12	Digital microscopic images of ECT constructs stained with Masson's trichrome stain and varying concentrations of CNTs (0.025%, 0.050% and 0.100%), images 1-3, respectively or graphene (0.005%, 0.010% and 0.020%), images 1-3, respectively: A) Control (3T3 cells without treatment); B) SWCNTs-Py-OH; C) SWCNTs-Py-COOH; D) MWCNTs-Py-OH; E) MWCNTs-Py-COOH; F) Graphene-Py-OH and G) Graphene-Py-COOH. Blue stain is for collagen, red/pink is for cellular cytoplasm and black is for CNTs or graphene.	61
3.13	Histopathological analysis of ECT constructs of 3T3 cells with different A) CNTs loading or B) graphene loading. The symbols * and # indicate significance ($P \leq 0.05$) with respect to control (0.000%) and the highest graphene loading (0.020%), respectively. The statistical significance was determined by two-way ANOVA. The extent of fibrosis was digitally quantified by the "color deconvolution" plugin in ImageJ.	62
3.14	SEM images at 5 μ m for 3T3 cells treated with different concentrations of CNTs (0.025%, 0.050% and 0.100%), images 1-3, respectively or graphene (0.005%, 0.010% and 0.020%), images 1-3, respectively: A) Control (3T3 cells without treatment); B) SWCNTs-Py-OH; C) SWCNTs-Py-COOH; D) MWCNTs-Py-OH; E) MWCNTs-Py-COOH; F) Graphene-Py-OH and G) Graphene-Py-COOH.	65

3.15	SEM evaluation of ECT constructs of 3T3 cells with different A) CNTs loading or B) graphene loading. The symbol * indicates significance ($P \leq 0.05$) with respect to control (0.000%). The statistical significance was determined by two-way ANOVA. Collagen fiber thickness was digitally quantified by ImageJ.	66
3.16	SEM evaluation analysis of ECT constructs of 3T3 cells with different A) CNTs loading or B) graphene loading. The symbol * indicates significance ($P \leq 0.05$) with respect to control (0.000%). The statistical significance was determined by two-way ANOVA. Matrix porosity was digitally quantified by ImageJ.	67
3.17	Images of ECT constructs contraction with varying CNTs or graphene loading: A) Control (Primary skin fibroblasts); B) SWCNTs-Py-OH (0.050%); C) MWCNTs-Py-OH (0.050%) and D) Graphene-Py-OH (0.010%).	69
3.18	The ECT constructs of primary skin fibroblasts with varying CNTs or graphene loading diameter measurements. The symbol * indicates significance ($P \leq 0.05$) with respect to control. The statistical significance was determined by Student t-test.	70
3.19	Average electrical conductivity of ECT constructs of primary skin fibroblasts with different CNTs loading or graphene loading. The symbol * indicates significance ($P \leq 0.05$) with respect to control. The statistical significance was determined by Student t-test.	71
3.20	Digital microscopic images of ECT constructs stained with Masson's trichrome stain and varying CNTs or graphene loading: A) Control (Primary skin fibroblasts); B) SWCNTs-Py-OH (0.050%); C) MWCNTs-Py-OH (0.050%) and D) Graphene-Py-OH (0.010%). Blue stain is for collagen, red/pink is for cellular cytoplasm and black is for CNTs or graphene.	72
3.21	Histopathological analysis of ECT constructs of primary skin fibroblasts with different CNTs loading or graphene loading. The symbol * indicates significance ($P \leq 0.05$) with respect to control (0.000%). The statistical significance was determined by Student t-test. The extent of fibrosis was digitally quantified by the "color deconvolution" plugin in ImageJ.	73
3.22	SEM images at 5 μm for varying CNTs or graphene loading: A) Control (Primary skin fibroblasts); B) SWCNTs-Py-OH (0.050%); C) MWCNTs-Py-OH (0.050%) and D) Graphene-Py-OH (0.010%).	74

3.23	SEM evaluation of ECT constructs of primary skin fibroblasts with different CNTs loading or graphene loading. There is no significance ($P \leq 0.05$) with respect to control (0.000%). The statistical significance was determined by Student t-test. Collagen fiber thickness was digitally quantified by the “color deconvolution” plugin in ImageJ.	75
3.24	SEM evaluation of ECT constructs of primary skin fibroblasts with different CNTs loading or graphene loading. The symbol * indicates significance ($P \leq 0.05$) with respect to control (0.000%). The statistical significance was determined by Student t-test. Matrix porosity was digitally quantified by the “color deconvolution” plugin in ImageJ.	76

List of Schemes

NO.	Scheme Title	Page
1	Noncovalent functionalization of SWCNTs with (A) Py-OH, (B) Py-COOH.	25
2	Noncovalent functionalization of MWCNTs with (A) Py-OH, (B) Py-COOH.	26
3	Noncovalent functionalization of graphene with (A) Py-OH, (B) Py-COOH.	27
4	Synthesis of Py-TEG-triazole-TEG-OH (6) and Py-TEG-triazole-TEG-COOH (7).	48
5	Non-covalent functionalization of carbon nanomaterials.	49

List of Abbreviations

Symbol	Abbreviation
CDCl ₃	Deuteriochloroform
CHCl ₃	Chloroform
CNTs	Carbon nanotubes
COOH	Carboxylic acid
DCM	Dichloromethane
DMAP	4-Dimethylaminopyridine
DMEM	Dulbecco's Modified Eagle's Medium
DMSO	Dimethylsulfoxide
ECM	Extracellular matrix
ECTs	Engineered connective tissues
EDC	1-Ethyl-3-(3-dimethylaminopropyl)carbodiimide hydrochloride
Et ₃ N	Trimethylamine
FBS	Fetal bovine serum
<i>f</i> -graphene	Functionalized graphene
<i>f</i> -MWCNTs	Functionalized multi-walled carbon nanotubes
<i>f</i> -SWCNTs	Functionalized single-walled carbon nanotubes
FTIR	Fourier-transform infrared spectroscopy
GO	Graphene oxide
H ₂	Hydrogen gas
H ₂ O	Water
HCl	Hydrochloride
MeOH	Methanol
MTS	3-(4,5-dimethylthiazol-2-yl)-5-(3-carboxymethoxyphenyl)-2-(4-sulfophenyl)-2H-tetrazolium
MW	Molecular weight
MWCNT	Multi-walled carbon nanotube
NaHCO ₃	Sodium bicarbonate
NaOH	Sodium hydroxide
Na ₂ SO ₄	Sodium sulfate
NMR	Nuclear Magnetic Resonance
°C	Degree Celsius
OH	Hydroxyl
PALS	Phase analysis light scattering
PBS	Phosphate buffer saline
Pen-Strep	Penicillin-streptomycin
PFA	Paraformaldehyde
pH	Power of hydrogen

PLGA	poly(lactic-co-glycolic acid)
p-graphene	Pristine graphene
p-MWCNTs	Pristine multi-walled carbon nanotubes
<i>p</i> -SWCNTs	Pristine single-walled carbon nanotubes
SEM	Scanning electron microscope
SWCNT	Single-walled carbon nanotubes
TEG	Tetraethylene glycol
TEM	Transmission electron microscope
TGA	Thermogravimetric analysis
THF	Tetrahydrofuran
TLC	Thin layer chromatography
UV-vis	Ultraviolet-visible
w/v	Weight by volume

Noncovalent Functionalization of Carbon Nanomaterials as a Scaffold for Tissue Engineering

By

Sahar Eyad Alhaj Qasem

Superviseors

Dr. Mohyeddin Assali

Dr. Naim Kittana

Abstract

Tissue engineering is one of the hot topics in recent research that needs especial requirements that depends on the developed scaffold to achieve a successful tissue growth. Various progress was achieved to develop the adequate biomaterials that provide a good scaffold with the optimum porosity, mechanical and electrical properties. In the recent years, considerable attention has been given to carbon nanomaterials and collagen composite materials and their applications in the field of tissue engineering.

However, carbon nanomaterials suffer from low water solubility which hampered their utilization. Therefore, we aimed to functionalize carbon nanomaterials non-covalently with pyrene moiety and using an appropriate hydrophilic linker -a derivative of polyethylene glycol- to disperse the carbon nanostructures in water. This non-covalent functionalization will preserve the electronic properties of the carbon nanostructure to be as a suitable scaffold for tissue engineering. These functionalized carbon nanomaterials were characterized by transmission electron microscopy (TEM). TEM images exhibited good dispersibility of the functionalized carbon nanomaterials with a diameter range of (5-15) nm for *f*-CNTs and (0.6-0.8) μm for *f*-graphene. Also, the successful π - π stacking between the

pyrene moieties and the carbon nanostructures was confirmed by absorption spectra. Moreover, thermogravimetric analysis (TGA) was used to quantify the amount of functionalization of the used carbon nanomaterials which is in the range of (17-29) %. Finally, zeta potential analysis was used obtaining in all cases around -20 mV that indicates the formation of a stable suspension.

3T3 cells-based engineered connective tissues (ECTs) were generated with different concentrations of carbon nanomaterials. Developed tissues showed a significant enhancement in the electrical conductivity that was mostly kind-dependent. While in ECTs containing primary skin fibroblasts showed lower electrical conductivity. 3T3 cells viability was confirmed by MTS assay and the data demonstrated that the concentrations 0.025% of CNTs and 0.005% of graphene derivatives reduced the cell viability between around (10-30) %. These concentrations were found to be enough to significantly enhance the electrical conductivity of the tissues. All tested tissues significantly decreased the tissue fibrosis relative to the control tissues except the 0.020% graphene-Py-COOH which exhibited a degree of fibrosis that was similar to that of the control ECT. The thickness of collagen fibers in all conditions were similar to that of the control except the 0.005% graphene-Py-COOH which exhibited a statistically significant reduction. All developed ECTs exhibited statistically significantly decrease in matrix porosity relative to the control. While in ECTs containing primary skin fibroblasts all ECTs of CNTs and graphene loadings did not exhibit any statistically significant change on collagen fiber thickness

relative to the control. Taken together with the conductivity data it can be assumed that the porosity of the ECT does not correlate with the conductivity of the tissues.

Chapter one

Introduction

1.1 Carbon allotropes

Carbon is an element in the periodic table that plays a basic role in nature (1). Carbon element forms numerous allotropes (figure 1.1) (2), such as graphite and diamond which are natural and known since ancient times, carbon nanotubes (CNTs) and fullerenes (Buckyball) which are synthetic allotropes and discovered in 10-20 years ago and graphene which are also synthetic and was only gained very recently (1, 3).

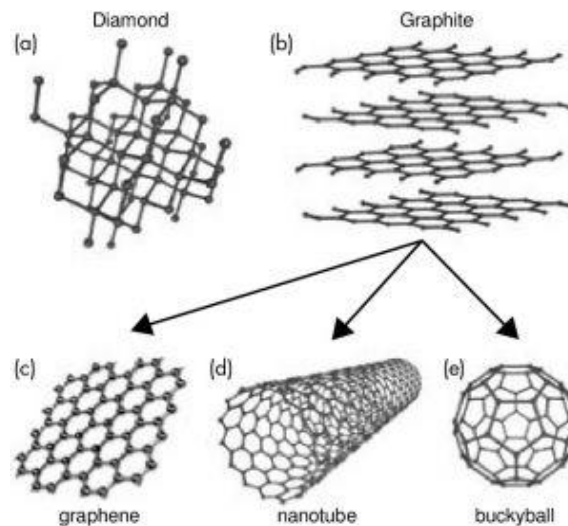


Figure 1.1: Some carbon allotropes (2).

CNTs and graphene are some of the most heavily searched carbon nanomaterials by the scientific community because of their unique properties (thermal and electrical conductivities and superior mechanical properties) (4).

1.1.1 Carbon nanotubes

CNTs have been studied largely in many specializations including physics, chemistry, biology, medicine and engineering because of their unique nanostructure, special properties and promising applications (5, 6). CNTs can be described as a graphene sheet made of condensed benzene rings and rolled up into a seamless tubule with diameters range between 1-100 nm and length in the range of micrometers (7, 8). There are two main types of CNTs: single-walled carbon nanotubes (SWCNTs) which is only a single sheet of graphene rolled up, or multi-walled carbon nanotubes (MWCNTs) which are formed of more than one sheet of graphene (9). (Figure 1.2) (10).

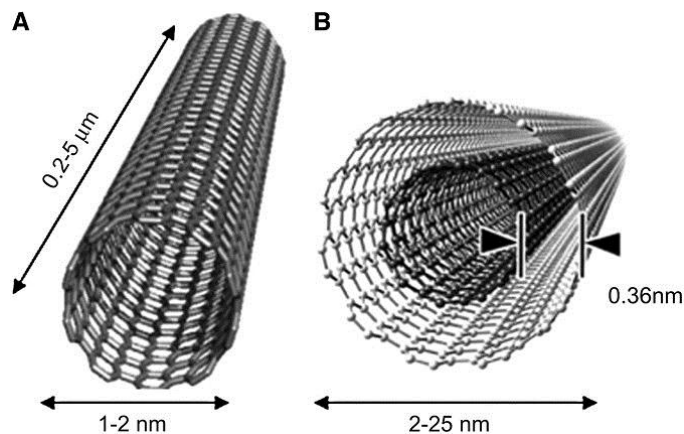


Figure 1.2: A) SWCNTs; B) MWCNTs (10).

CNTs show a special one-dimensional hollow shape and excellent mechanical, electrical and thermal properties (11). CNTs have a significant large surface area depending on their nano-dimensions (12). They are highly porous and lightweight materials (13). They also can be metallic or semiconducting according to the arrangement of their rings over the tubular surface (14). All these properties make them a powerful promising material

for biomedical applications, such as drug and gene delivery, biomedical imaging, biosensors for biomolecules, tissue engineering and regenerative medicine (15). CNTs are a substantial substance in tissue engineering due to imparting unique properties to the scaffold and steering cell growth. They can sense and increase cellular behavior, tracking and labeling cells and enhancing tissue matrices (16).

1.1.2 Graphene

Since graphene detection, it has attracted researchers from different fields to explore its possibilities in various applications. They considered it a super material because of its unique nanostructure and exceptional properties (17). Graphene is a two-dimensional honey-comb monolayer of graphite with a C-C bond length of 0.142 nm (figure 1.3) (4, 18, 19).

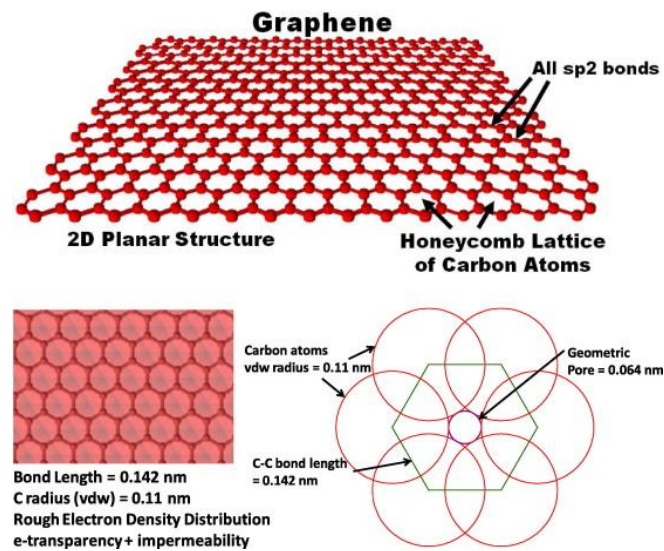


Figure 1.3: Graphene structure (19).

The unique structure of graphene offers noticeable physical properties such as high mechanical strength, high electrical and thermal conductivity and high carrier mobilities (20). Graphene also has a very large surface area to volume ratio (21). In addition, graphene has excellent stability and ultrahigh sensitivity. All these superb properties make graphene an attractive promising material for biomedical applications, such as biosensors, biomedical devices, drug delivery, cancer therapy and tissue engineering (17). Graphene is utilized as scaffolding in tissue engineering, these scaffolds have excellent mechanical properties which enabled proper adhesion, sustained proliferation and enhanced differentiation of various cells in tissue engineering applications (22).

1.2 Functionalization of CNTs and graphene

Poor solubility of CNTs and graphene in most organic solvents and aqueous solutions adversely affects their use in biological applications. So a suitable functionalization on the surface of CNTs and graphene can improve their water solubility, biocompatibility and thus decrease their toxicity (23, 24). There are two major protocols for the functionalization of CNTs and graphene: covalent reactions and noncovalent reactions (23-25).

1.2.1 Covalent functionalization

Covalent reactions occur between functional groups generated during chemical reactions on the π -conjugated skeleton of carbon nanomaterials (25). This protocol has been known to disrupt the π -network of carbon

nanomaterials leading to potential loss of their electrical and mechanical properties (26). The purpose of this protocol of functionalization is to block the release of the attached biomolecules before attaining the target site and decrease the side effects of these biomolecules. This great stability of covalently functionalized CNTs and graphene is preferable in drug delivery (27).

1.2.1.1 Covalent functionalization of CNTs:

There are many reported successful covalent surface functionalization (figure 1.4) (5). The two general strategies of covalent functionalization that lead to biomedical applications are: nonselective attack of nanotube sidewalls using very reactive species like nitrenes (28) and aryl diazonium salts (29, 30) and the second strategy is the formation of amide bond at ends of nanotubes using carboxyl group which usually can be generated on CNTs by oxidation in strong acid (25, 28).

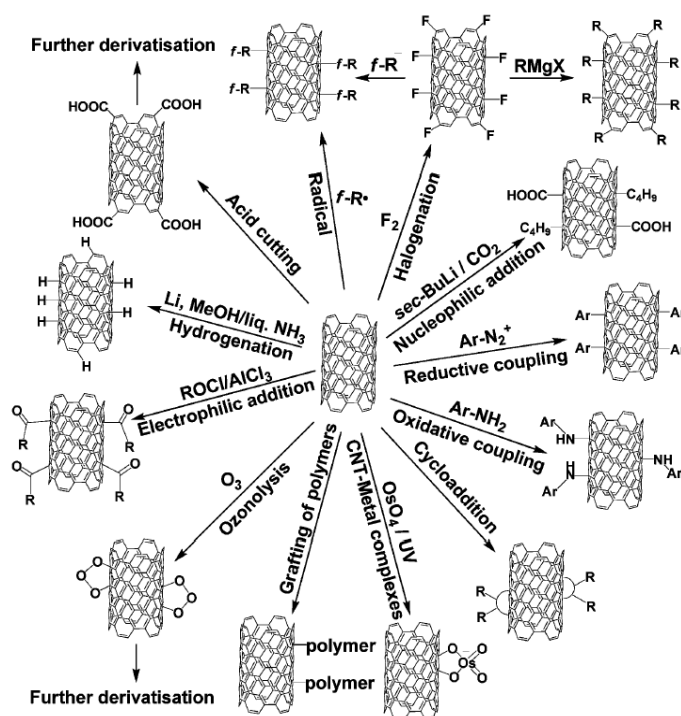


Figure 1.4: Covalent functionalization of CNTs (5).

1.2.1.2 Covalent functionalization of graphene:

There is various covalent functionalization chemistry of graphene (figure 1.5) (31). These functionalization can be achieved in two different ways: either by using the carboxyl groups of graphene oxide (GO) through ester or amide formation (32) or by direct reaction with the graphene sheet which includes free radical addition reaction (33), nucleophilic substitution reaction (34) and Cycloaddition reaction (35).

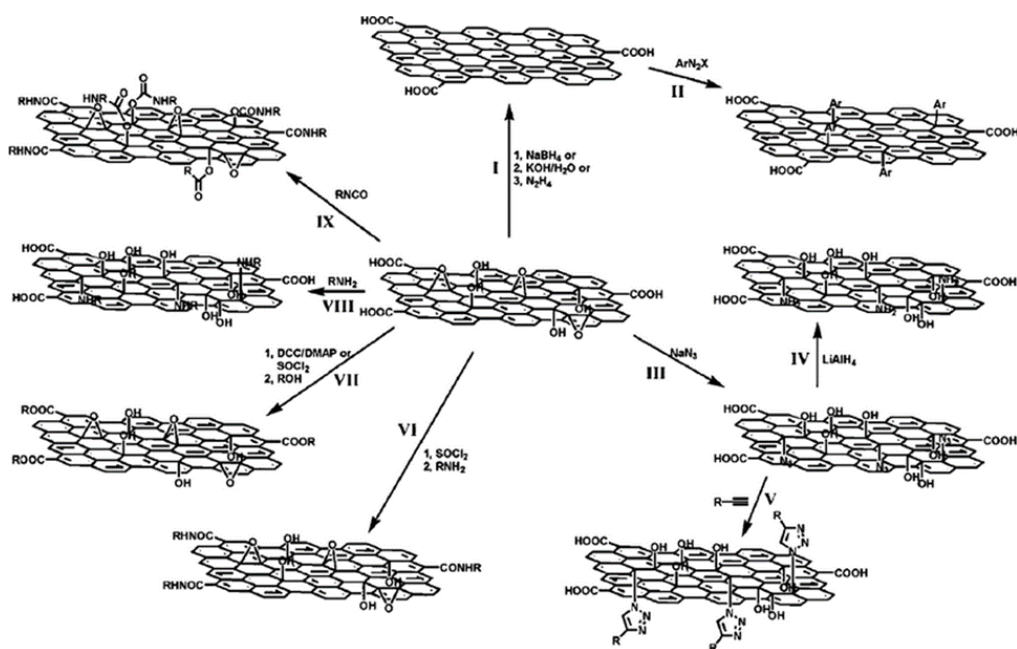


Figure 1.5: Covalent functionalization of graphene. I: Reduction of GO into graphene. II: Covalent surface functionalization of reduced graphene via diazonium reaction. III: Functionalization of GO by the reaction between GO and sodium azide. IV: Reduction of azide–GO with LiAlH_4 . V: Functionalization of azide–GO through click chemistry. VI: Modification of GO with long alkyl chains by the acylation reaction. VII: Esterification of GO by DCC chemistry or the acylation reaction. VIII: Nucleophilic ring-opening reaction. IX: The treatment of GO with organic isocyanates leading to the derivatization of both the edge carboxyl and surface hydroxyl functional groups via formation of amides or carbamate esters (31).

1.2.2 Non-covalent functionalization

Noncovalent reactions occur via π – π stacking, van der Waals force or electrostatic interaction. This route can be achieved by entrapment such as, entrap the CNTs or graphene in biocompatible polymer or by physical adsorption of suitable molecules such as surfactants, phospholipids and peptides (24, 25).

1.2.2.1 Non-covalent functionalization of CNTs:

The first general and straightforward approach for the functionalization of SWCNTs with proteins via π - π stacking was announced by Dai and co-workers (36). 1-pyrenebutanoic acid, succinimidyl ester which is a bifunctional molecule, was adsorbed irreversibly onto the sidewall of SWCNTs via π - π stacking between SWCNTs sidewall and the pyrenyl group (figure 1.6). Then, proteins were immobilized by anucleophilic substitution of *N*-hydroxysuccinimide through the amino group of the proteins to form an amide bond (36).

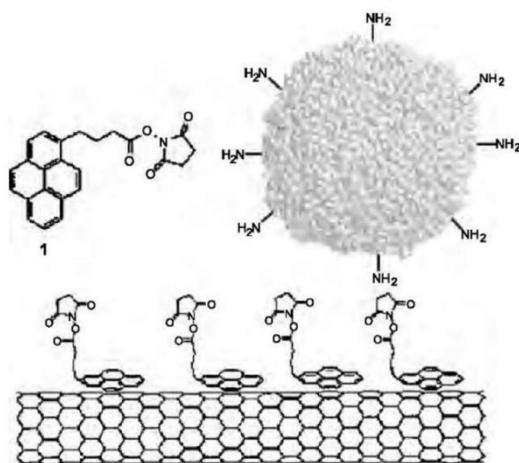


Figure 1.6: Noncovalent adsorption of single-walled carbon nanotube with 1-pyrenebutanoic acid, succinimidyl ester via π - π stacking (36).

In another study, an efficient approach for the functionalization of MWCNTs noncovalently with neogly-coconjugates via π - π stacking was developed by Assali and co-workers (26). This approach was established on the utilize of sugar-based amphiphiles functionalized with tetrabenzo[*a,c,g,i*]fluorene (Tbf) which is a polyaromatic compound and it is topology beats a butterfly with open wings (figure 1.7). Also, it has been

established to upgrade the weak capability of pyrene-based systems to exfoliate MWCNTs in water (26).

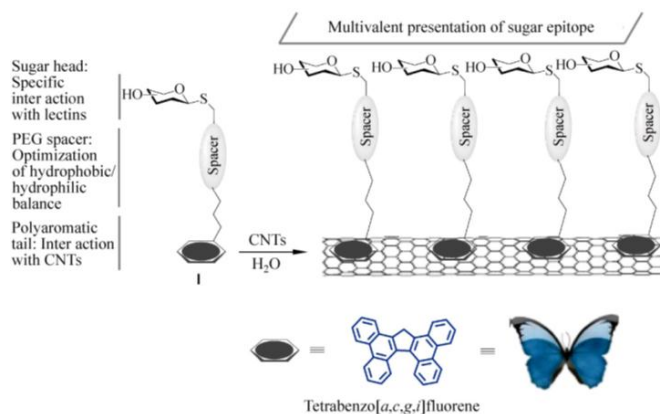


Figure 1.7: Schematic representation of the synthesis of the Tbf-linked carbohydrate-MWCNTs (26).

1.2.2.2 Non-covalent functionalization of graphene:

The first example for the concoction of stable aqueous dispersion of polymer-coated graphene nanoparticles was reported by Stankovich et al. (37). They functionalized the graphene noncovalently using an exfoliation/in-situ method to reduce graphite oxide in the existence of poly(sodium 4-styrenesulfonate) (PSS) (37). Another example of the functionalization of graphene noncovalently with pyrene derivatives via π - π stacking was reported by Xu and co-workers (38). They successfully did a noncovalent functionalization of reduced graphene oxide using 1-pyrenebutyrate which is a stabilizer with a strong affinity toward the basal plane of graphene via π - π stacking. The obtained functionalized graphene is highly dispersed in water and has exhibited an electrical conductivity which is 7 orders of magnitude bigger than that of GO precursor (38).

Another example of the functionalization of graphene noncovalently by coating the surface of graphene with polymers through van der Waals forces was reported by Suslick et al. (39). They used the sonochemical method to functionalize graphene begins with styrene reactive monomer and receiving polystyrene functionalized graphene. The presence of styrene with the ultrasonic irradiation exfoliated the graphene sheets to monolayers of graphene flakes. Also, the radical polymerization of styrene has formed polystyrene on the surface of graphene flakes. The obtained graphene exhibited huge solubility in different organic solvents such as DMF, chloroform and toluene (39).

The non-covalent route and in contrast to the covalent route can maintain the sp^2 nanotube structure, π -conjugated structure and so the electronic characteristics and other optical properties of CNTs and graphene (23-25, 36, 40). So, preserving the physical properties of CNTs and graphene using the noncovalent route make them favorable for nerve and tissue engineering (41, 42).

1.3 Regenerative medicine

Regenerative medicine is a relatively new multidisciplinary field of science that aims to restore, preserve or reinforce tissues and so organ functions for patients with injury and/or diseases by regenerating cells, tissues and organs (43, 44). The improvement in the discovery of cell biology, biological molecules and biomaterial science have led to new options for tissue and organ engineering (45). Diseases, such as Alzheimer's disease,

Parkinson's disease, spine injuries, osteoporosis or cancer might be soon treated with modes that aim to regenerate damaged or diseased tissue (43). While the accelerated in the clinical use of regenerative medicine technologies the pharmacological sciences will critically contribute to that. In 2017, the "regenerative pharmacology" phrase was coined to represent the huge possibilities that could happen at the interface between regenerative medicine, pharmacology and tissue engineering (46).

1.3.1 Regenerative pharmacology

Regenerative pharmacology is a general term and has been defined as "the application of pharmacological sciences to accelerate, optimize, and characterize (either *in vitro* or *in vivo*) the development, maturation, and function of bioengineered and regenerating tissues" (46). Regenerative medicine is a challenging field in drug development which seeks to modify tissue and organ physiology to improve functional outcomes by utilizing chemokine, particular growth factor or drug to trigger a specific response in a tissue (figure 1.8) (46-48).

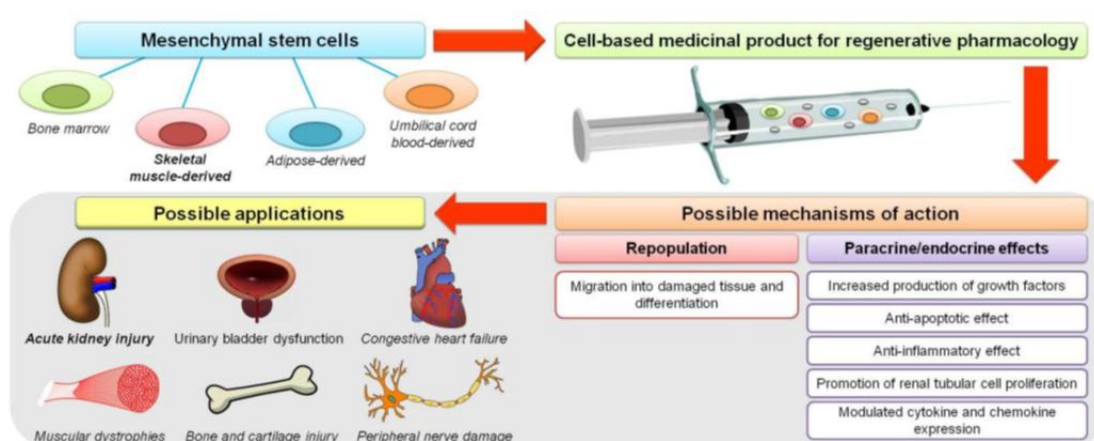


Figure 1.8: General scheme for regenerative pharmacology (47).

For example, CXCL12 (SDF-1 α) which is a regenerative pharmacologic factor was examined for its impact on the myocardial regeneration by Schuh and co-workers. They displayed that cells overexpressing SDF-1 promote myocardial regeneration (49, 50). Song *et al.* also reported about the regeneration of chronic myocardial infarction. They injected hydrogels containing angiogenic peptide Ac-SDKP and stem cell homing factor SDF-1 (51).

1.3.2 Tissue engineering

Tissue engineering term was introduced in 1987 through a National Science Foundation meeting. It was defined as the application of principles and methods of engineering in life sciences by specifying a field of multidisciplinary research that purpose to improve active biological substitutes qualified for maintaining and/or restoring normal tissue function (52). Tissue engineering is one of the main ingredients of regenerative medicine which have the bases of materials engineering and cell

transplantation to develop biological substitutes that can maintain and/or restore tissue normal function (53). It has two general categories, the first which is depending on natural ability of the body to regenerate for right direction and orientation of new tissue growth by using acellular matrices which are prepared usually by making artificial scaffolds or through removing the cellular components from tissues by chemical and mechanical manipulation to make collagen-rich matrices (54, 55). The second category which is the *in vivo* regeneration or the *in vitro* generation by using scaffolds made of natural or synthetic materials and filled with living cells (figure 1.9) (43, 56). The presence of a porous scaffold with biomolecules that appropriate for the objected cells and the entrapment of nanoparticles could reinforce greatly the success of the tissue engineering strategy (43, 57).

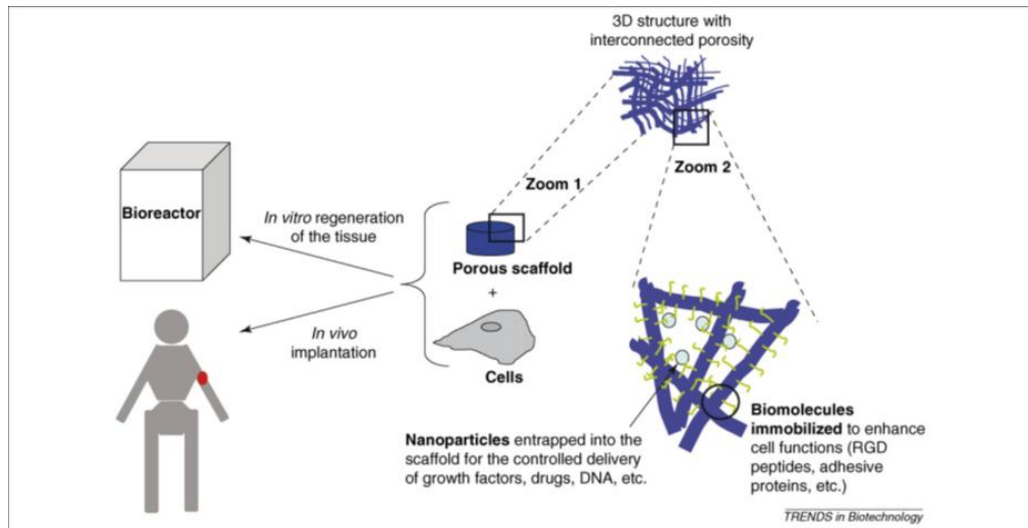


Figure 1.9: Tissue engineering approach for tissue regeneration (43).

One of the essential components for tissue engineering is the extracellular matrix (ECM) which is the non-cellular component that exists in all tissues (58, 59). The natural ECM is formed of proteoglycans, signaling molecules, adhesion proteins and collagen. This environment which surrounds all cells is fundamental for the normal function of tissues and is also crucial for the regeneration of these tissues when any pathology or damage happens because it helps the cells to move, growth, adhesive, proliferate and differentiate. So, the eligible synthetic ECM should identify as close as to the natural ECM to enable tissue engineering (52, 58). One of the most common biological materials to make a synthetic ECM is collagen, which is an abundant protein that exists in the ECM in body tissues and it can supply binding sites to support cells to adhesive, migrate, proliferate and also differentiate (60, 61).

These body tissues which are related but not identical cells that are joined and work together to achieve specific functions are composed of four main types: epithelial tissue that has a protective function and composes the outer layer of the body and lines many of the body cavities, muscle tissue which is presented in the body in three types smooth, skeletal and cardiac and all are able to contract and forms various movement whether voluntary or involuntary, nerve tissue which is subdivided into central and peripheral and involved in the carrying of chemical and electrical impulses from the central nervous system and brain to the periphery and vice versa and the last tissue is connective tissue which is a biological tissue that is exist in almost every organ and compositing a huge part of blood vessels, joints,

tendons, ligaments, muscles and skin (62-64). Connective tissue supports and as the name implies connects other tissues. This tissue is important for, cell migration, wound healing, mechanical support and controlling metabolic processes in other tissues and so the properties of the connective tissue unlike the properties of other tissues which primarily depend on their cellular elements. There are various types of connective tissue with loose and dense connective tissue are the most common. All types of connective tissues are made of cells which are mainly fibroblasts, fibers as collagen and ECM but the type of intracellular matrix varies according to the type of connective tissue (64). Unfortunately, some connective tissue injuries are a common clinical challenge because of the limited inherent repair capacity and hence was the need to develop a scaffold that maintains normal tissue function (65, 66). One of the roadblocks in this developed scaffold is the inability to imitating the properties of the natural tissues and this challenge was solved by insertion of customized nanoparticles in these scaffolds (67, 68).

One of the most common nanoparticles utilized in scaffolds is carbon nanomaterial which has features that is mutual with that of the natural ECM such as elasticity, flexibility and porosity with similar diameters (42, 69-71). So, the combination of carbon nanomaterials with their remarkable physical properties using collagen as a biomaterial is being studied as suitable scaffolds to optimize tissue regeneration (42). Another remarkable property of carbon nanomaterial is electrical conductivity. This

property is responsible for enhancing electrical coupling between the cells and thus an improvement in connective heart tissue engineering (69, 72).

In the end, functionalized CNTs and graphene can act as useful nanomaterials for tissue regeneration applications (90, 91). The functionalized carbon nanomaterial can be combined with polymeric hydrogels, such as collagen, to form novel scaffolds that mimic as much as possible the composition and properties of the ECM and thus optimizing cell growth in injured tissue (42, 90, 92, 93). These scaffolds incorporate the favorable properties of both collagen and functionalized carbon nanomaterial. They are bioresorbable, biodegradable, biocompatible, have the desired mechanical rigidity and electrical conductivity and maintaining porous three-dimensional nanostructure (90). The sum of these properties allows the desired cells to attach the scaffold surface to proliferate and differentiate (42). These unique scaffolds become able to promote the regeneration of different tissue types, such as skin and myocardium (42, 94).

1.4 Literature Review

Many efforts were carried out in order to synthesize a suitable scaffold for tissue engineering using different types of carbon allotropes such as SWCNTs, MWCNTs and graphene. It is clear from our perspective of knowledge that there are no previous reports that study the noncovalent functionalization of carbon nanomaterials as a scaffold for connective and cardiac tissue engineering. In this literature review, some attempts to

improve tissue engineering science using SWCNTs, MWCNTs and graphene were mainly reported.

In 2005, Macdonald *et al.* prepared composite materials containing a collagen matrix with implanted CNT (figure 1.10) (95). They mixed solutions of carboxylated SWCNTs at different concentrations with solubilized collagen type I. When collagen gelation, living smooth muscle cells were inserted to produce composite matrices of cell-seeded collagen-CNT. Constructs enclousing the highest concentration of CNT marked delayed gel compaction, comparative to lower concentration which compacted at the same ratio as pure collagen controls. In all constructs, the cell viability at both days 3 and 7 was consistently above 85%, while cell number in constructs containing CNT was lower than in collagen controls constructs at day 3, and statistically not varied by day 7. Scanning electron microscopy (SEM) exhibited physical interaction through the collagen matrix and CNT. Raman spectroscopy confirmed the presence of CNT but did not show strong molecular interactions through the CNT and collagen matrices. The results showed that this collagen-CNT matrices could have advantage to be scaffolds for tissue engineering (95).

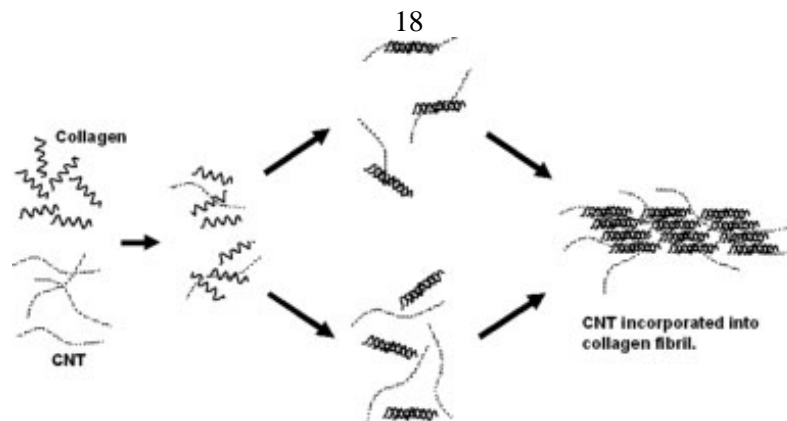


Figure 1.10: Schematic of process by which CNT can be incorporated into collagen fibrils (95).

Three years later, collagen-SWCNT composite with human dermal fibroblast cells (HDF) implanted directly in the matrix was developed by Stegemann and co-workers from the Department of Biomedical Engineering, Rensselaer Polytechnic Institute, New York, (figure 1.11) (93). They polymerized type I solubilized collagen in the presence of dispersed SWCNTs and HDF cells to obtain constructs with different SWCNTs concentration. Then, they evaluated the electrical properties at days 3 and 7 which was increased uniformly with increasing SWCNTs concentrations. All the matrices of SWCNTs-Collagen hydrogel subjected HDF-mediated gel compaction by time, but the rate and extent of gel compaction were decreased significantly because of the presence of SWCNTs. The cell morphology was not affected by SWCNTs and cell viability was coordinately high in all constructs. However, at day 7 cell number decreased with increasing SWCNTs loading. The results showed that these composite biomaterials could be applicable as scaffolds for tissue engineering (93).

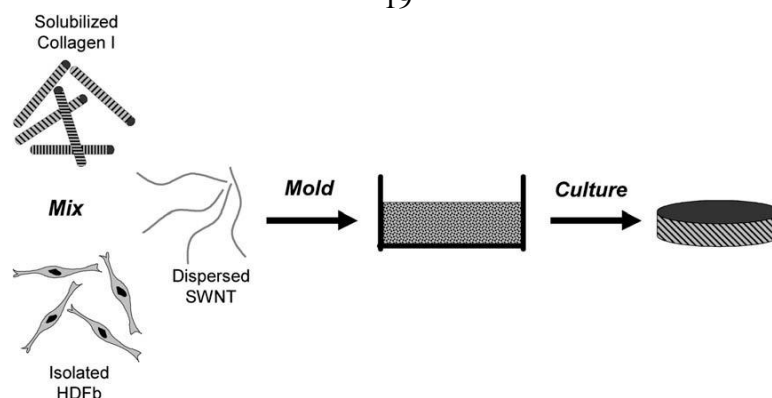


Figure 1.11: Schematic diagram of the construct preparation process (93).

In 2014, Mikael *et al.* improved the mechanical strength of poly(lactic-co-glycolic acid) (PLGA) microsphere scaffolds by structuring it with CNTs so that these scaffolds may be usable for regeneration applications and load-bearing repair (96). They have created microspheres scaffolds of PLGA which consist of pristine and modified (with carboxylic acid (COOH) and hydroxyl (OH)) MWCNTs and molded them into three-dimensional porous scaffolds. outcomes showed that when only adding 3% MWCNTs, the modulus and compressive strength were increased significantly compared with pure PLGA scaffolds. SEM images appeared perfect cell adhesion and proliferation. While *in vitro* studies on osteoblast-like MC3T3-E1 cells showed good cell viability, mineralization and proliferation. However, the *in vivo* study on 28 male rats marked variations in inflammatory response in the 12 weeks of implantation, where OH-MWCNTs had the lowest response, while pristine MWCNTs and COOH-MWCNTs exhibited a more announced response. In total, the results demonstrated that PLGA scaffolds containing water-dispersed modified MWCNTs were mechanically more powerful and showed pretty tissue

compatibility, and so are potential candidates for bone tissue engineering (96). In another study published one year later, researchers from The Department of Biomedical Engineering, Stony Brook University, New York, reported the fabrication and cytocompatibility of three-dimensional chemically crosslinked macro-sized porous CNTs scaffolds (97). These scaffolds were made by radical initiated thermal crosslinking of SWCNTs and MWCNTs. MC3T3 preosteoblast cells exhibited good cell viability on SWCNTs and MWCNTs scaffolds comparable to PLGA scaffolds after 5 days. The immunofluorescence imaging and confocal live-cell displayed that MC3T3 cells could attach and proliferate on SWCNTs and MWCNTs scaffolds. While SEM imaging confirmed cell attachment and spreading and proposed that cell morphology is ruled by roughness of scaffold surface. So that, MC3T3 cells were rounded on scaffolds of low surface roughness (SWCNTs) and elongated on scaffolds of high surface roughness (MWCNTs). These outcomes elucidated that crosslinked SWCNTs and MWCNTs scaffolds are cyto-compatible and can open avenues to develop these scaffolds for tissue engineering applications (97). In 2016, myocardial tissue constructs of (reduced GO (rGO)-inserted gelatin methacryloyl (GelMA) hydrogels) were engineered by Tang and his collaborator (figure 1.12) (98). The presence of rGO in the GelMA hydrogel enhances the mechanical properties and electrical conductivity of the matrix significantly. Moreover, NIH-3T3 cells cultured on rGO-GelMA scaffolds displayed better cell viability, maturation and proliferation compared to those cultured on pure GelMA hydrogels. Primary

cardiomyocytes of neonatal rats exhibited faster and stronger spontaneous beating rate on rGO-GelMA scaffolds compared to ones on pure GelMA hydrogel. The results expected that these scaffolds could be applied broadly in future biomaterial designs to upgrade tissue engineering outcomes (98).

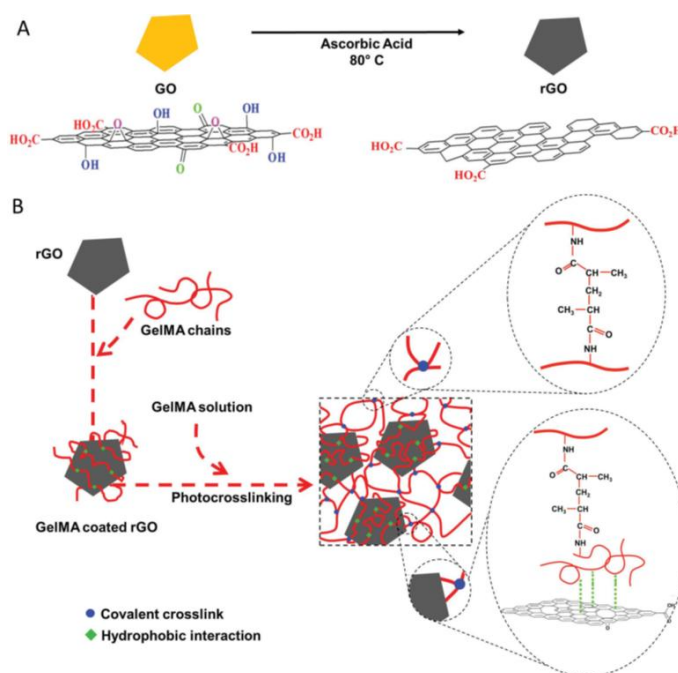


Figure 1.12: Schematic illustration of the rGO-GelMA synthesis process. A) Process of producing rGO from GO using ascorbic acid; B) Preparation procedure of rGO-GelMA hybrid hydrogels (98).

In another study published one year later, Sun *et al.* fabricated a myocardial tissue construct of SWCNTs-Collagen hydrogels (CNT-Col) (figure 1.13) (99). the integration of SWCNTs improved electrical and mechanical properties. These SWCNTs (up to 1 wt%) showed no toxicity to Neonatal rat ventricular myocytes (NRVMs) and enhanced cell elongation and adhesion. While the transmission electron microscopy (TEM), histology test and intracellular calcium-transient measurement exhibited that the

integration of SWCNTs remarkably improved cell alignment, and so an engineered cardiac tissue with stronger contraction potential was formed. The results suggested that such a scaffold could be applicable soon, as injectable biomaterials to submit drug molecules or cells for cardiac regeneration after myocardial infarction (99).

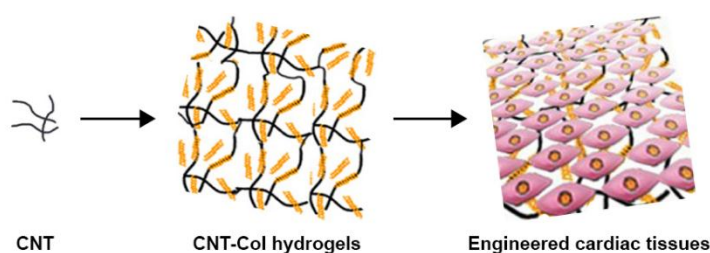


Figure 1.13: Schematic representation to describe the study (99).

1.5 Aims of the study

The aim of this project is to functionalize the CNTs and graphene non-covalently with the appropriate balance in order to study their suitability as a scaffold for tissue engineering.

1.6 Objectives

- 1) Synthesis of various pyrene derivatives to develop the adequate derivative for the functionalization of carbon nanomaterials.
- 2) Noncovalent functionalization of CNTs and graphene and study the dispersibility and stability.

- 3) Characterization of the functionalized carbon nanomaterials with the various analytical techniques.
- 4) Preparation of carbon nanomaterials/Collagen hydrogels constructs.
- 5) Assess the properties of the formed carbon nanomaterials/Collagen hydrogels constructs, including rigidity, stability, porous three-dimensional nanostructure and electrical conductivity of constructs.
- 6) Assess the biocompatibility of the formed constructs.

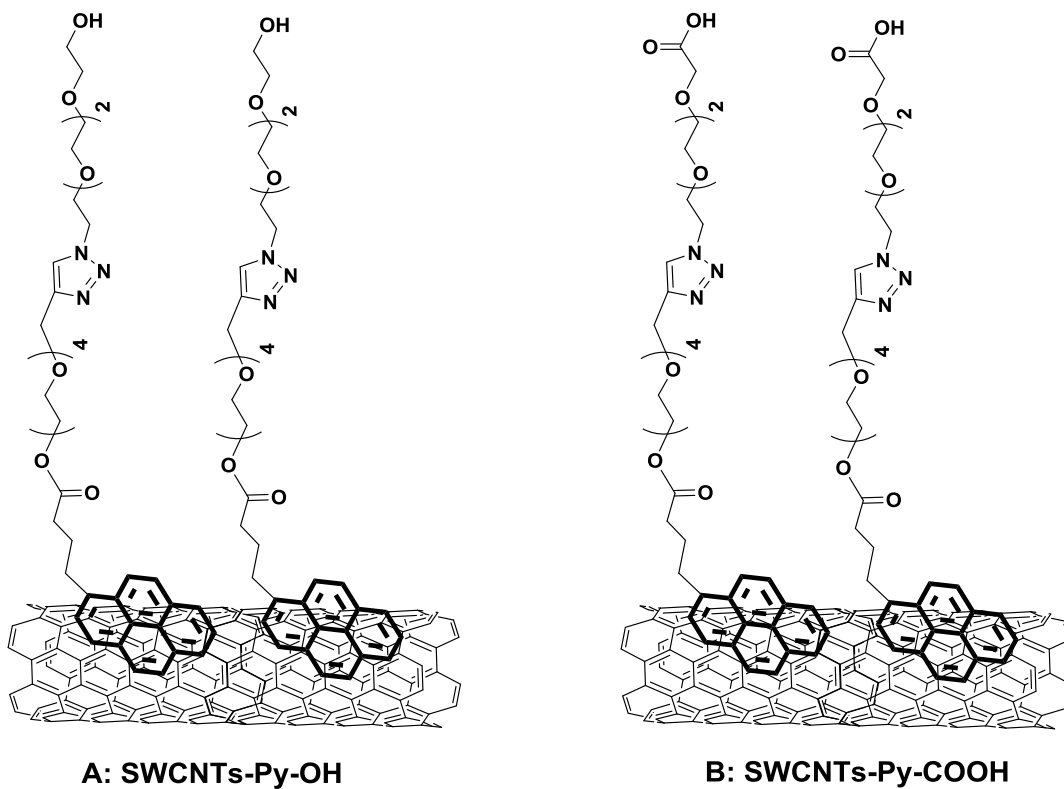
1.7 The importance of this project

While tissue and organ repair and replacement are a critical healthcare matter all over the world. Regenerative medicine displays the opportunity to regenerate damaged or diseased tissue (44). And so, diseases such as Alzheimer's disease, Parkinson's disease, spine injuries, osteoporosis, cancer or cardiovascular diseases might be soon treated (43, 83). However, the interest in applying nanotechnology to regenerative medicine is rising because of its ability to generate scaffolds with nanostructures that are capable to mimic natural tissues (43). One of the most common nanomaterials utilized in scaffolds is carbon nanomaterial which has features and remarkable properties that are mutual with that of the natural ECM (42, 69). Poor solubility of CNTs and graphene in most organic solvents and aqueous solutions adversely affects their use in biological applications. So a suitable functionalization on the surface of CNTs and graphene can improve their water solubility, biocompatibility and thus

decrease their toxicity (23, 24). In this project we aim to functionalize the carbon nanomaterials non-covalently in order to preserve the electronic properties of the carbon nanostructure to be as a scaffold for tissue engineering. We used a hydrophilic linker to obtain the adequate hydrophobic/hydrophilic balance that capable to disperse the carbon nanostructures in water. This hydrophilic linker was synthesized with a terminal hydroxyl or carboxyl functional group to study the effect of these groups on the tissue formation and electrical behavior of the formed tissue. Many efforts were carried out in order to synthesize a suitable scaffold for tissue engineering using different types of carbon allotropes such as SWCNTs, MWCNTs and graphene. It is clear from our perspective of knowledge that there are no previous reports that study the noncovalent functionalization of carbon nanomaterials as a scaffold for connective and cardiac tissue engineering.

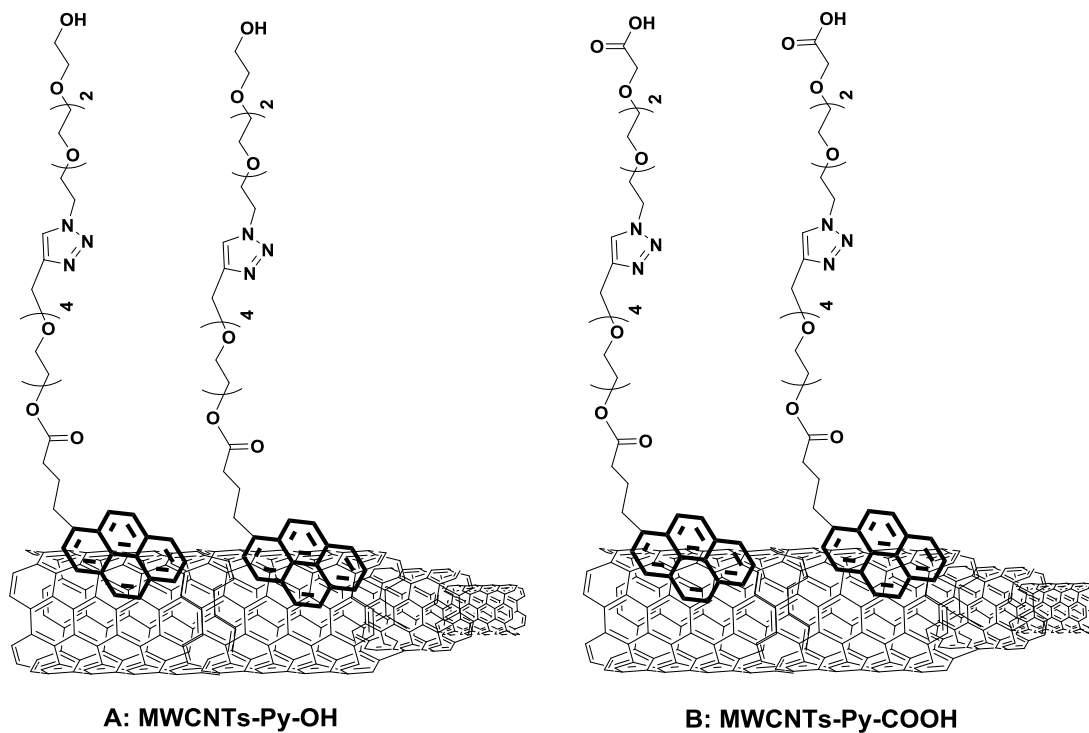
1.8 General approach of the synthesis and functionalization of CNTs and graphene

Scheme 1 illustrates the noncovalent functionalization of SWCNTs with pyrene-OH and pyrene-COOH.



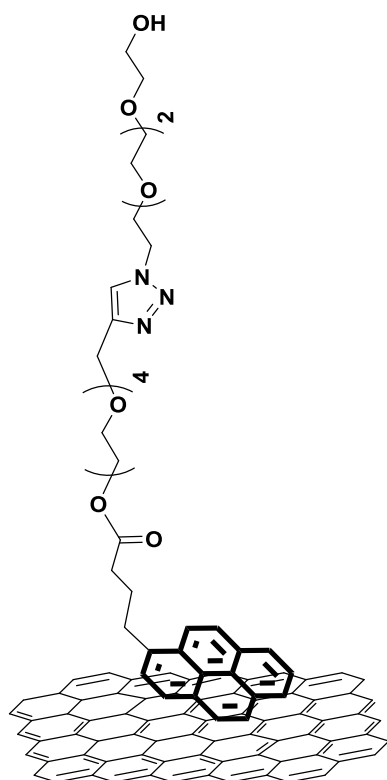
Scheme 1: Noncovalent functionalization of SWCNTs with (A) Py-OH and (B) Py-COOH.

Scheme 2 illustrates the noncovalent functionalization of MWCNTs with pyrene-OH and pyrene-COOH.

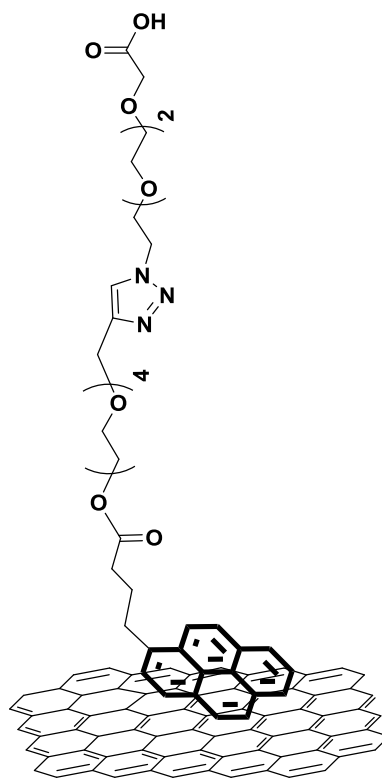


Scheme 2: Noncovalent functionalization of MWCNTs with (A) Py-OH and (B) Py-COOH.

Scheme 3 illustrates the noncovalent functionalization of graphene with pyrene-OH and pyrene-COOH.



A: Graphene-Py-OH



B: Graphene-Py-COOH

Scheme 3: Noncovalent functionalization of graphene with (A) Py-OH and (B) Py-COOH.

Chapter Two

Methodology

2.1 Reagents and materials

All reagents and materials utilized in the experiments were of analytical grade. L-ascorbic acid sodium salt (Catalog # A17759), 1-(3-Dimethylaminopropyl)-3-ethylcarbodiimide hydrochloride (EDC) (catalog # A10807), propargyl bromide (Catalog # A16580), tetraethylene glycol (TEG) (Catalog # B23990) and 1-Pyrenebutyric acid (Catalog # A17760) were purchased from (Alfa Aesar company, England).

Sodium azide (Catalog # 0E30428) was purchased from (Riedel de Haën Company, Germany). 4-(dimethylamino) pyridine (DMAP) (Catalog # 1122583), tetrahydrofuran anhydrous (Catalog # 186562-2L) and anhydrous copper sulfate (Catalog # 451657) were purchased from (SIGMA-ALDRICH, USA). Acetone, ethanol (EtOH), methanol (MeOH), isopropyl alcohol and dichloromethane (DCM) were purchased from (C.S. Company, Haifa). Chloroform (CHCl_3) (catalog # 67-66-3), triethylamine (Et_3N) (Catalog # 40502L05) and diethyl ether (catalog # 38132) were purchased from (Merck Millipore). Ethyl acetate (EtOAc) (Catalog # 2355516100024) and n-hexane (Hex) (Catalog # 2355544800024) solvents were purchased from (Frutarom Company, Haifa). Tetrahydrofuran (THF) solvent (Catalog # 487308) was purchased from (Carlo Erba Company, MI, Italy). Sodium hydroxide and sodium chloride were purchased from (C.S. Company, Haifa). Sodium hydrogen carbonate was purchased from

(Al-Zahra Factory Co. Palestine). Short SWCNTs (Catalog # 1246-022514), MWCNTs (Catalog # 1235-041709) and graphene (Catalog # 2191-072413) were purchased from (Nanostructured & Amorphous Materials, Inc USA).

All reactions were stirred beneath ambient conditions. Column chromatography utilizing silica gel (pore size 60 Å) purchased from (Sigma Aldrich Company) was utilized to purify the products. TLC (DC-Fertigfolien ALUGERAM[®]SIL G/UV254, MACHEREY NAGEL Company, Germany) was utilized to monitor the reactions. Centrifuge (UNIVERSAL 320, Hettich Zentrifugen, Germany) and water bath sonicator (MRC DC-200H Digital Ultrasonic Cleaner) were utilized in the preparation and dispersion of functionalized CNTs and graphene. Rotary evaporator (MRC, ROVA-100, laboratory equipment manufacturer) was utilized for solvents drying.

For the biological test, Dulbecco's free Ca⁺⁺ -phosphate-buffered saline (REF # 02-023-1A), DMEM (REF # 01-055-1A) and L-glutamine solution (REF # 03-020-1B) were purchased from (Biological industries, Jerusalem). Trypsin-EDTA solution 1X (Catalog # 59417C), fetal Bovin Serum (catalog # C8065), trypan blue solution (Catalog # RNBD6249), DMEM powder (Catalog # 56436C-10L) and collagen solution from bovine skin (Catalog # C4243-20ML) were purchased from (SIGMA-ALDRICH, USA). Celltiter 96[®] Aqueous one solution cell proliferation Assay (Catalog # G3580) was purchased from (Promega, USA).

2.2 Instrumentation

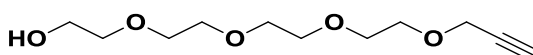
- **Ultraviolet-Visible (UV-VIS) spectra** were measured using 10-mm quartz cuvettes in (7315 Spectrophotometer, Jenway, UK).
- **Zeta potential** was measured in NanoBrook Omni (Brookhaven Instruments, USA).
- **Electrical conductivity** was captured utilizing Four Probe Method AL-212 (Acumen labware, Ambala, India).
- **Fourier-transform infrared spectroscopy (FTIR)** was done on Nicolet iS5 (Thermo Fisher Scientific Company, USA).
- **Nuclear Magnetic Resonance (NMR) spectra** were obtained using Bruker Avance (500 spectrometers, Switzerland).
- **Thermogravimetric analysis (TGA) spectra** were recorded in the range 0-600 °C, flow rate 20 °C under nitrogen (100 cc/min) by (STA 409 PC luxx[®], NETZSCH).
- **Transition electron microscope (TEM)** images were taken at 60 kV using Morgagni 286 transmission microscope (FEI Company, Eindhoven, Netherlands).
- **Scanning electron microscope (SEM)** images were done on Versa 3D (FEI Company, Eindhoven, Netherlands).

- **Digital microscope** images for histopathological evaluation were done on Leica ICC50 HD (Leica camera AG company, Wetzlar, Germany).
- **Esco celculture CO₂ incubator** was used to incubate the cell line.
- **Accumax Variable micropipette** which made in UK was used in pipetting.
- **Unilab microplate reader 6000** was utilized in the cell viability test to read the plate.

2.3 Synthesis and characterization of the products

All the synthetic procedures were conducted at An-Najah University labs. NMR, SEM, TEM and TGA measurements were run at the University of Jordan.

2.3.1 Synthesis of OH-TEG-alkyne, compound (1)



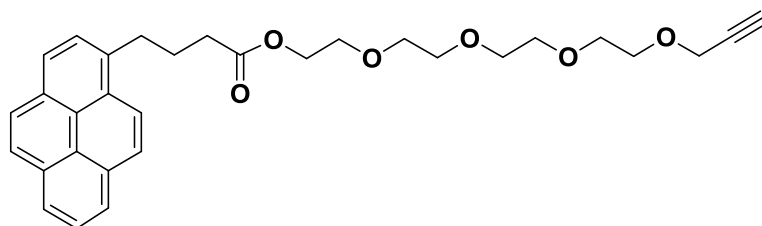
TEG (3 g, 15.4 mmol) was dried under vacuum and was dissolved in anhydrous THF (20 mL) under argon. In another round bottom flask, sodium hydride (NaH) (741 mg, 30.9 mmol) was dried under vacuum and was dissolved in anhydrous THF (10 mL) under argon. NaH solution was added to TEG solution dropwise until the hydrogen gas (H₂) was released. After that, propargyl bromide (1.9 mL, 21.6 mmol) was dried under vacuum and was dissolved in anhydrous THF (10 mL) under argon and was added to the reaction. The reaction was vigorously stirred overnight at

room temperature. The next day, water (H₂O) (5 mL) was added to the reaction drop by drop and the reaction was evaporated. The crude product was extracted by DCM (100 mL) then it was dried by Na₂SO₄, filtered and evaporated. The product was purified by silica column chromatography in ethyl acetate to obtain an oily yellow product with a yield of (1.7 g, 7.3 mmol, 47.4 %).

R_f: 0.46 (Ethyl acetate).

¹H NMR and ¹³C NMR were obtained as in the literature (100).

2.3.2 Synthesis of Pyrene-TEG-alkyne, compound (2)



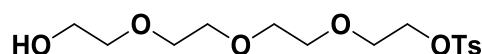
Compound (1) (1 g, 4.3 mmol), pyrenebutyric acid (620.7 mg, 2.2 mmol), 1-Ethyl-3-(3-dimethylaminopropyl) carbodiimide hydrochloride (EDC) (1.2 g, 6.5 mmol) and 4-Dimethylaminopyridine (DMAP) (396.2 mg, 3.2 mmol) were dissolved in DCM (20 mL) and were reacted under argon. The reaction was vigorously stirred for 24 hours at room temperature. The crude product was extracted by DCM (170 mL) and 1 M HCL (50 mL) then it was dried by Na₂SO₄, filtered and evaporated. The product was purified by silica column chromatography in ethyl acetate/n-hexane (1:2) to obtain an oily yellow product with a yield of (980 mg, 1.9 mmol, 44.2%).

R_f: 0.57 (Ethyl acetate/n-Hexane (1:1)).

¹H NMR (500 MHz, CDCl₃): δ 8.29-7.83 (m, 9H, Py), 4.23 (s, 2H, CH₂OCO), 4.15 (s, 2H, OCH₂C≡CH), 3.67-3.53 (m, 14H, 7CH₂O), 3.37 (t, 2H, *J* = 7.2 Hz, Py-CH₂), 2.47 (t, 2H, *J* = 7.2 Hz, CH₂COO), 2.39 (s, 1H, C≡CH), 2.20-2.15 (quint, 2H, Py-CH₂CH₂).

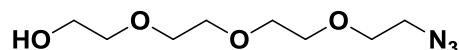
¹³C NMR (125.7 MHz, CDCl₃): δ 173.5, 135.8, 131.4, 130.9, 130.0, 128.7, 127.5, 127.4, 126.7, 125.9, 125.1, 125.0, 124.9, 124.8, 123.4, 72.5, 70.5, 70.4, 70.2, 69.7, 69.2, 69.1, 64.6, 63.5, 61.6, 61.5, 61.0, 33.8, 32.7, 29.7, 26.8.

2.3.3 Synthesis of OH-TEG-Tosyl, compound (3)



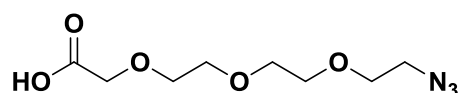
The compound was synthesized and identified as in the literature (101).

2.3.4 Synthesis of OH-TEG-N₃, compound (4)



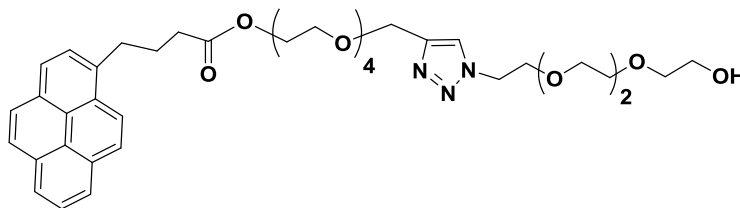
The compound was synthesized and identified as in the literature (102).

2.3.5 Synthesis of COOH-TEG-N₃, compound (5)



The compound was synthesized and identified as in the literature (102).

2.3.6 Synthesis of Pyrene-TEG-triazole-TEG-OH, compound (6)



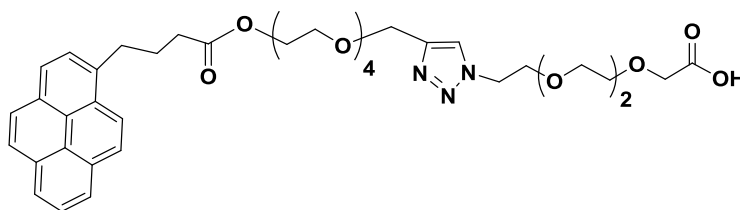
Compound **(2)** (296.5 mg, 0.6 mmol) and compound **(4)** (194 mg, 0.9 mmol) were dissolved in DCM (8 mL) and a solution of sodium ascorbate (233.7 mg, 1.2 mmol) and anhydrous copper sulfate (188.3 mg, 1.2 mmol) in H₂O (8 mL) was added. The reaction was vigorously stirred for 24 hours at room temperature. The product was extracted by DCM (160 mL) and H₂O (50 mL) then it was dried by Na₂SO₄, filtered and evaporated. The product was purified by silica column chromatography in DCM/MeOH (20:1) to obtain an oily yellow product with a yield of (260 mg, 0.4 mmol, 66.7 %).

R_f: 0.57 (DCM/MeOH (20:1)).

¹H NMR: (500 MHz, CDCl₃): δ 8.22-7.78 (m, 9H, Py), 7.68 (s, 1H, CH triazole), 4.62 (s, 2H, CH₂-triazole), 4.39 (t, 2H, *J* = 4.9 Hz, CH₂OCO), 4.20 (t, 2H, *J* = 4.8 Hz, CH₂N), 3.69 (t, 2H, *J* = 4.9 Hz, CH₂OH), 3.65-3.42 (m, 26 H, 13CH₂O), 3.32 (t, 2H, *J* = 7.6 Hz, CH₂CO), 2.43 (t, 2H, *J* = 7.4 Hz, Py-CH₂), 2.13 (quint, 2H, Py-CH₂CH₂).

^{13}C NMR (125.7 MHz, CDCl_3): δ 173.4, 135.7, 131.4, 130.9, 130.0, 128.7, 127.5, 127.4, 126.7, 125.9, 125.1, 125.0, 124.9, 124.8, 124.0, 123.3, 72.7, 70.5, 70.4, 70.2, 69.6, 69.3, 69.1, 64.5, 63.5, 61.6, 50.2, 33.8, 32.7, 29.7, 26.8.

2.3.7 Synthesis of Pyrene-TEG-triazole-TEG-COOH, compound (7)



To a solution of compound (2) (287.3 mg, 0.6 mmol) and compound (5) (200 mg, 0.9 mmol) in DCM (8 mL) a solution of sodium ascorbate (226.5 mg, 1.1 mmol) and anhydrous copper sulfate (182.5 mg, 1.1 mmol) in H_2O (8 mL) was added. The reaction was vigorously stirred for 24 hours at room temperature. The product was extracted by DCM (160 mL) and H_2O (50 mL) then it was dried by Na_2SO_4 , filtered and evaporated. The product was purified by silica column chromatography in DCM/MeOH (20:1) to obtain an oily yellow product with a yield of (180 mg, 0.2 mmol, 33.3%).

R_f : 0.49 (DCM/MeOH (20:1)).

^1H NMR: (500 MHz, CDCl_3): δ 8.29-7.83 (m, 9H, Py), 7.76 (bs, 1H, triazole), 4.63 (s, 2H, CH_2COOH), 4.58 (s, 2H, $\text{CH}_2\text{-triazole}$), 4.49 (t, 2H, $J = 5.0$ Hz, CH_2OCO), 4.22 (t, 2H, $J = 4.8$ Hz, CH_2N), 3.82 (t, 2H, $J = 4.9$ Hz, triazole- CH_2CH_2), 3.68-3.55 (m, 22H, 11 CH_2O), 3.37 (t, 2H, $J = 7.7$

Hz, CH₂CO), 2.47 (t, 2H, $J = 7.3$ Hz, Py-CH₂), 2.11 (quint, 2H, Py-CH₂CH₂).

¹³C NMR (125.7 MHz, CDCl₃): δ 173.5, 170.4, 135.8, 131.4, 130.9, 130.0, 128.7, 127.5, 127.4, 126.7, 125.9, 125.1, 125.0, 124.9, 124.8, 123.4, 70.9, 70.5, 70.4, 69.7, 69.3, 69.2, 69.0, 68.5, 64.6, 63.7, 63.6, 63.5, 53.5, 33.8, 32.8, 29.7, 26.8.

2.4 Optimization of the needed amount of compound (6) or (7) to functionalize SWCNTs, MWCNTs and graphene in H₂O

Different quantities of compound (6) or (7) (0.25, 0.5, 1 mg) were dissolved in H₂O (1 mL) then 1 mL of SWCNTs, MWCNTs or graphene were added up to the solution and sonicated for 30 minutes. After that, the different dispersions were preserved under observation to study the optimum concentration needed to disperse the carbon nanomaterials in water without the formation of any precipitation or excess of micellar structures in the TEM images.

2.5 Connective tissues casting and characterization

2.5.1 Generation of engineered connective tissues (ECTs)

2.5.1.1 Normal DMEM growth medium preparation

Fetal bovine serum was added to basal DMEM high glucose medium so that the concentration of FBS would be 10% for culturing 3T3 cells or 15% for culturing primary skin fibroblasts. Generally, 1% L-glutamine and 1%

antibacterial penicillin-streptomycin (Pen-Strep) were added to the DMEM growth medium.

2.5.1.2 2x DMEM preparation

The intention here was to prepare a growth DMEM medium that contains double concentration of each constituent (2x DMEM) (87). The approach was to fortify the normal DMEM growth medium with further amounts DMEM powder, NaHCO_3 powder, serum and antibiotics that could be otherwise used to prepare 1x DMEM growth medium in distilled water. To prepare (20 mL) of 2x DMEM, (17 mL) of the growth DMEM medium was added in a beaker on a stirrer. This liquid medium already contains 1x DMEM powder, 1x NaHCO_3 , 1x FBS and 1x Pen-Strep as described above. Then, (267.2 mg) of DMEM powder was added slowly to the beaker and mixed to around 30 minutes. After that, (74 mg) NaHCO_3 was added and stirred until fully dissolved then the pH was adjusted to (6.9-7.1) by using 1N sodium hydroxide (NaOH) or 1N HCl. Also, (2 mL) FBS and (200 μL) of 1% Pen-Strep were added in order to double the concentration of these constituents in the medium. After that, the volume was completed to (20 mL) using liquid DMEM and then was sterile filtered by using a sterile syringe filter and hence the 2x DMEM is ready to use.

2.5.1.3 Preparation of sterile 0.1 N NaOH for tissue generation

NaOH (40 mg) was dissolved in distilled H_2O (10 mL) and then it was filtered using a membrane filter.

2.5.1.4 Stock solutions preparation

2.5.1.4.1 SWCNTs-OH, MWCNTs-OH, SWCNTs-COOH and MWCNTs-COOH

Eight mg of each CNTs species were separately dissolved in 1x phosphate buffer saline (PBS) (192 μ L), then they were sonicated for 2 hours to get a dispersion of 4% concentration. After that, they were autoclaved to become sterilized, and the evaporated water was later compensated.

2.5.1.4.2 Graphene-OH and graphene-COOH

Eight mg of each of the graphene species was dissolved separately in 1x PBS (768 μ L) and then they were sonicated for 2 hours and got a dispersion with a concentration of 1%. After that, they were autoclaved to become sterilized and the evaporated water was later compensated.

2.5.1.5 Cell suspension preparation

2.5.1.5.1 3T3 cells

3T3 cells were cultured in T-75 culture flask in DMEM growth medium (20 mL) which contains 10% FBS, 1% L-glutamine and 1% Pen-Strep. The culture flasks were maintained in a cell culture incubator that was adjusted to 37 °C and 5% CO₂. When the cells grew and became almost 90% confluent, they were sub-cultured as follows. First the medium was suctioned, and the cells were washed by 1x PBS (15 mL). Then 0.05% trypsin (3 mL) was added up to cells and the flask was incubated in the

incubator (37 °C, 5% CO₂) for 5 minutes while most of the cells detached from the surface of the flask. At this point, trypsin was inactivated by the addition of the growth DMEM medium (20 mL) and the cell suspension was collected in a sterile falcon tube. The cells were counted and thereafter centrifuged to precipitate the cells in the bottom of the falcon tube. The supernatant medium was carefully suctioned and fresh growth DMEM medium was added to get the desired concentration of cells (57.1×10^6 cell/mL).

2.5.1.5.2 Primary skin fibroblasts

Neonatal mice 1-3 days age were euthanized by cervical dislocation and then they were sterilized using povidone-iodine solution and 70% ethanol. After that, the skin was removed under the hood and washed with 1x PBS several times. The skin was minced by sterilized surgical operation blade into (1mm) piece size, then it was incubated with 0.25% trypsin in the incubator (37 °C, 5% CO₂) for 10 minutes with gentle shaking while incubation. Then, the cell suspension was taken and DMEM medium (20 mL) which contains 15% FBS, 1% L-glutamine and 1% Pen-Strep was added up to it, this procedure was run 3 times and then the cell suspension was cultured in T-75 culture flask for several days with medium changing every 2 days. At the same time, skin residues were placed on the surface of T-75 culture flask with dermis layer facing the surface and were left until partially dried so that they adhere to the surface. After that, growth DMEM medium (contains 15% FBS) was added carefully until it almost covers the

skin residue. The flask was left in the incubator (37 °C, 5% CO₂) for 10 days to allow the cells to grow, with medium changing every 2 days. After that, the cells were sub-cultured by the standard method explained before. The cells were counted and then centrifuged to precipitate the cells in the bottom of the falcon tube, the medium was suctioned and fresh growth DMEM medium (contains 15% FBS) was added to get the desired concentration of cells (57.1×10^6 cell/mL).

2.5.1.6 Preparation of engineered connective tissues (ECTs)

The composition for a single ECT (around 255 µL volume) is shown in (table 1). All the used constituents were kept at 4°C and were kept cold throughout the experiment. Each of the made ECT contained about 2.5×10^6 cells, 2x DMEM, collagen (3 mg/mL) and PBS, which they were all mixed in a pre-cooled Eppendorf tube in an ice box. After that the pH was titrated with 0.1 N NaOH until the color of the mixture became pink. Next, the cell suspension was added up to the Eppendorf and the mixture was cast in 48 well plate, which was previously coated with 7% gelatin. The plate was left at room temperature under the laminar flow hood for 15 minutes after which it was transferred to the incubator (37 °C, 5% CO₂), where it was incubated for further 25 minutes. At this point, a fresh DMEM growth medium was added and the plate was then kept in the incubator for 5 days with medium change every other day. The formula was scaled up according to the desired number of ECT to be prepared.

Table 1: The general composition of ECT.

Constituent	Volume (μL)
2x DMEM	100
Collagen (3 mg/mL)	100
PBS	6.3
NaOH (0.1 N)	~ 5
Cells suspension (57.1×10^6 cell/mL).	43.8
Total	~ 255

The different ECTs containing the different kinds of CNTs or graphene and they were prepared by the same protocol described above, but here instead of PBS we used an equivalent volume of a stock solution containing enough amount of CNTs or graphene that is required to achieve the target total concentration in the ECT master mix. The idea is to obtain ECTs with equal volume and because the graphene species have low density so the used concentrations of graphene species were smaller than CNTs species. In addition, when primary skin fibroblasts were used, the fresh growth DMEM medium contained 15% FBS, whereas for 3T3 cells the medium contained 10% FBS) (87).

2.5.2 Electrical conductivity of ECTs

All tissue samples were washed by PBS. After that, the voltage measurements were performed by changing the current values using the four-probe method and then the electrical conductivity was calculated (103). The four-point collinear probe is the most common route to measure the conductivity of a material. This method includes driving four evenly spaced probes in connect with the center of a material with unknown conductivity. The two outer probes are utilized for exporting current and

the two inner probes are utilized for measuring the outcoming voltage drop across the surface of the material (104). The conductivity σ can be calculated as $\sigma = 1/\rho$ where ρ is the resistivity and it can be calculated by $\rho = \rho_v/G7$ (W/S) hence G7 is a correction factor and it is a function of W which is the material thickness and S which is the distance between probes and ρ_v is the volume resistivity and it can be calculated by $\rho_v = V \times 2 \pi S/I$ where S is the distance between probes, I is the source current and V is the measured voltage (105).

2.5.3 Cell viability test

2.5.3.1 Cell culture

3T3 cells were cultured in T-75 culture flask in DMEM growth medium (20 mL) and they were incubated in the incubator (37 °C, 5% CO₂). When the cells were about 80-90% confluent they were collected by the trypsinization method described above. The cell suspension was adjusted so that the cell concentration is (1 x 10⁵ cell/mL). After that, the cell suspension was distributed into 96-well plate and they were left to adhere over 48 hours.

2.5.3.2 Stock solution preparation with serial dilutions

2.5.3.2.1 SWCNTs-OH, MWCNTs-OH, SWCNTs-COOH and MWCNTs-COOH

Two mg of each CNTs species was weighed on a piece of a clean aluminum foil then it was sterilized under UV light for 10 minutes and dissolved in DMEM growth medium (2 mL) to get a mixture with a concentration of 0.1% weight by volume (w/v) of each compound. After that, the mixtures were sonicated for 30 minutes and serially diluted as (1:1) so that 0.05% and 0.025% concentrations were generated. Finally, all the mixtures were sonicated for 1 hour.

2.5.3.2.2 Graphene-OH and graphene-COOH

Three point two mg of each of the graphene species was weighed on a piece of a clean aluminum foil then it was sterilized under UV light for 10 minutes and dissolved in DMEM growth medium (2 mL) to get a mixture with a concentration of 0.02% w/v of each compound. After that, the mixtures were sonicated for 30 minutes and serially diluted as (1:1) so that 0.01% and 0.005% concentrations were generated. Finally, all the mixtures were sonicated for 1 hour.

2.5.3.3 3-(4,5-dimethylthiazol-2-yl)-5-(3-carboxymethoxyphenyl)-2-(4-sulfophenyl)-2H-tetrazolium (MTS) assay

After 3T3 cells were sub-cultured into 96 well plate and left to adhere for 48 hours, the DMEM growth medium was taken off and the cells were incubated for 24 hours with (100 uL) of each of the working solutions prepared above. The plate contained 4 wells that were left without cells but with growth DMEM medium (blank samples) and 4 wells contained growth DMEM medium with cells (negative control). The treatment with each test condition (SWCNTs-OH, MWCNTs-OH, SWCNTs-COOHM, WCNTs-COOH, Graphene-OH and graphene-COOH) was made in quadruplicates. After that, MTS reagent (10 µL) was added up to every well and the plate was incubated in the incubator (37 °C, 5% CO₂). The absorbance at 492 nm was read every 30 minutes using a microplate reader until the absorbance of the control wells almost reached 1. At this point, the supernatant of each well was carried to a new empty tube for the measurement and the absorbance was read.

2.5.4 Histopathological evaluation for ECTs

All tissue samples were fixed in 4% paraformaldehyde (PFA) overnight and then they were kept in PBS at 4 °C. After that, these tissue samples were sectioned, processed and stained at the medical laboratory at An-Najah University Hospital according to the standard routine protocol followed for pathological samples. The tissue samples were stained by hematoxylin and eosin (H%E) stain and Masson's trichrome stain and then

they were examined by an independent-blinded clinical pathologist. In addition, the grade of fibrosis in the stained tissues was further analyzed digitally by ImageJ[®] software loaded with “color deconvolution” plugin.

2.5.5 SEM evaluation for ECTs

All tissue samples were fixed in 4% PFA overnight and then they were kept in PBS at 4 °C. After that, these tissue samples were frozen by liquid nitrogen and then they were fractured cryogenically using the surgical operation blade. These sections were dried on a stub and different pictures with different magnifications and resolutions were taken (106). Moreover, the pores size and the interaction between carbon nanomaterial and collagen were estimated digitally through analyzing the images by utilizing ImageJ[®] software.

2.5.6 Statistical evaluation for ECTs

The statistical analysis for electrical conductivity, cell viability, histopathological evaluation and SEM evaluation and the graphs were prepared by GraphPad Prism[®] software (GraphPad Software, La Jolla, CA, USA). Two-way ANOVA and Student’s t-test were used to compare the means.

Chapter Three

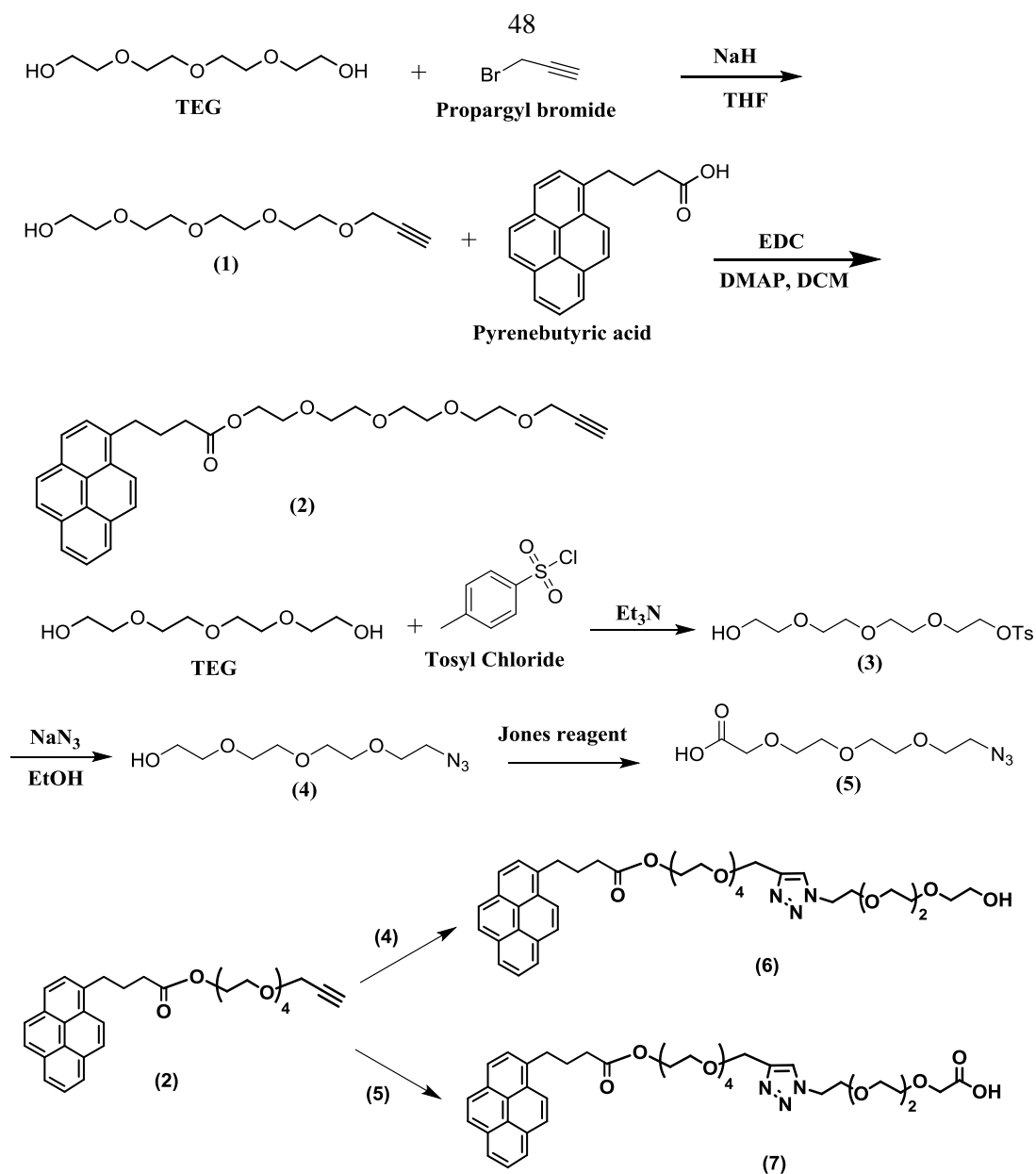
Results and Discussion

3.1 Synthesis and functionalization of carbon nanomaterials

3.1.1 Synthesis of Pyrene conjugates

In this project we aim to functionalize the carbon nanomaterials non-covalently in order to preserve the electronic properties of the carbon nanostructure to be as a scaffold for tissue engineering. For this purpose, we utilized the pyrene moiety to interact with the surface of the carbon nanostructures through π - π stacking (107). Moreover, the pyrene moiety was connected to a hydrophilic linker to obtain the adequate hydrophobic/hydrophilic balance that capable to disperse the carbon nanostructures in water. Therefore, in first place the hydrophilic linker was synthesized based on tetraethylene glycol derivative as shown in scheme 4. Herein, a double linker was synthesized with a terminal hydroxyl or carboxyl functional group to study the effect of these groups on the tissue formation and electrical behavior of the formed tissue. For this purpose, the reaction was begun by reacting TEG with propargyl bromide in the presence of sodium hydride to get the linker OH-TEG-alkyne (**1**). The synthesized linker was reacted with pyrenebutyric acid through esterification reaction using DMAP as a catalyst and EDC as a coupling agent to obtain Py-TEG-alkyne (**2**). On the other side and to synthesize the second linker, a selective tosylation reaction was conducted to TEG to get OH-TEG-OTs (**3**). Then, compound (**3**) was reacted with NaN_3 and hence

the tosyl group was replaced with azide in ethanol to get OH-TEG-N₃ (**4**). In order to obtain a carboxyl terminal, compound (**4**) was oxidized using Jones reagent to obtain COOH-TEG-N₃ (**5**). After that, OH-TEG-N₃ (**4**) or COOH-TEG-N₃ (**5**) was reacted with Py-TEG-alkyne (**2**) through click reaction (108). This click reaction was done using sodium ascorbate and anhydrous copper sulfate as catalysts dissolved in H₂O and DCM forming a triazole ring to synthesize Py-TEG-triazole-TEG-OH (**6**) or Py-TEG-triazole-TEG-COOH (**7**) as shown in scheme 4.

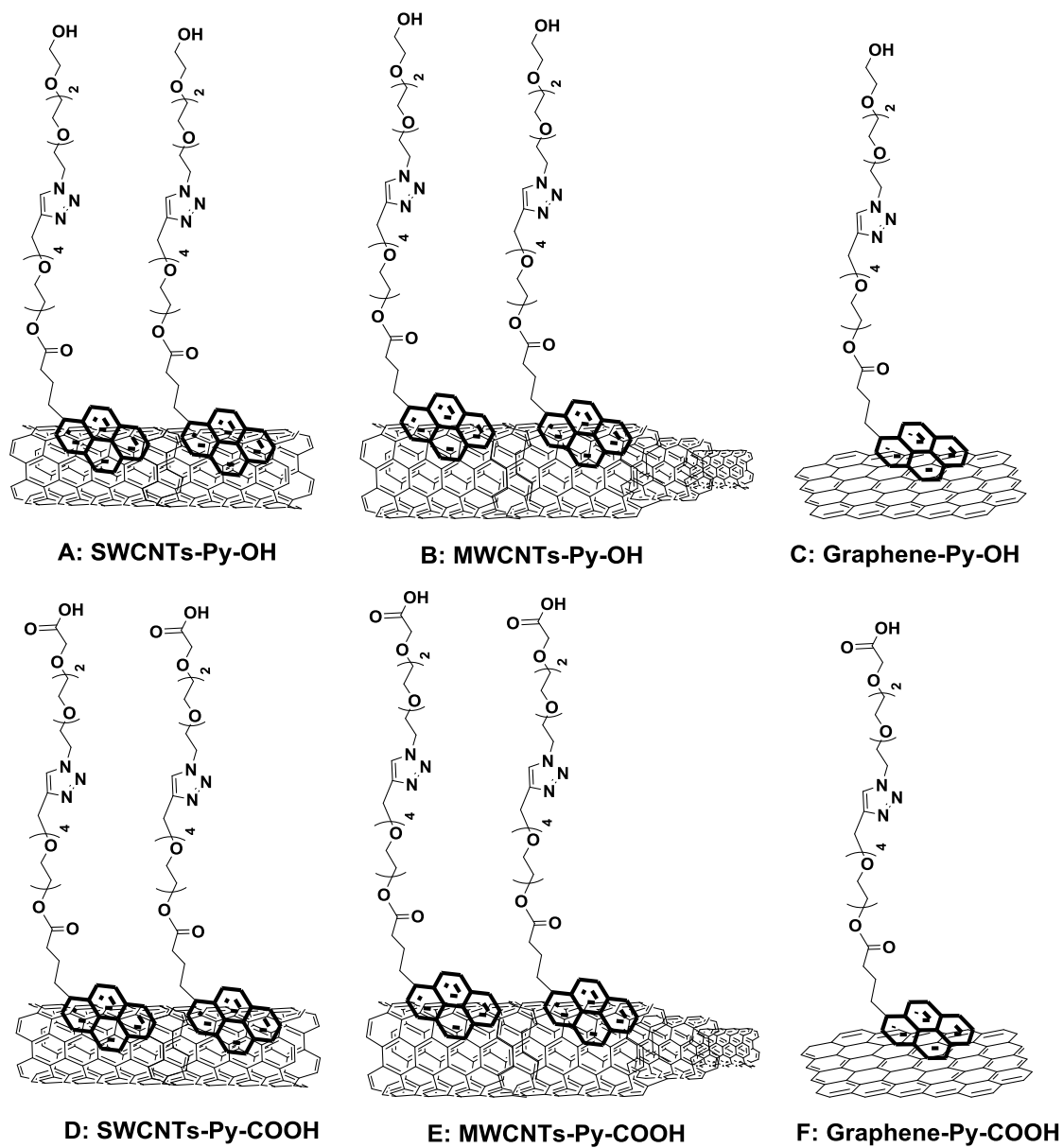


Scheme 4: Synthesis of Py-TEG-triazole-TEG-OH (**6**) and Py-TEG-triazole-TEG-COOH (**7**).

3.1.2 Non-covalent functionalization of carbon nanostructures

In order to optimize the required amount of compound (**6**) or (**7**) to functionalize the carbon nanomaterials noncovalently as shown in scheme 5. Various amounts (0.25, 0.5 and 1 mg/mL) were incubated with 1 mg of the carbon nanomaterials and sonicated for 30 minutes and study the dispersion and stability of the formed suspension. In all cases, the best-

needed amount was 0.5 mg/mL to functionalize the carbon nanostructures with good stability.



Scheme 5: Non-covalent functionalization of carbon nanomaterials.

3.2 Characterization of functionalized carbon nanomaterials

3.2.1 Dispersibility of the functionalized carbon nanomaterials

The dispersibility of functionalized SWCNTs, MWCNTs and graphene was performed. They displayed a good water dispersibility (figures 3.1, 3.2 and 3.3). Actually, p-SWCNTs, p-MWCNTs and p-graphene have low water dispersibility with rapid aggregation due to the hydrophobic characteristics. While, the functionalized SWCNTs (*f*-SWCNTs), MWCNTs (*f*-MWCNTs) and graphene (*f*-graphene) have increasing hydrophilicity and thus good water dispersibility.

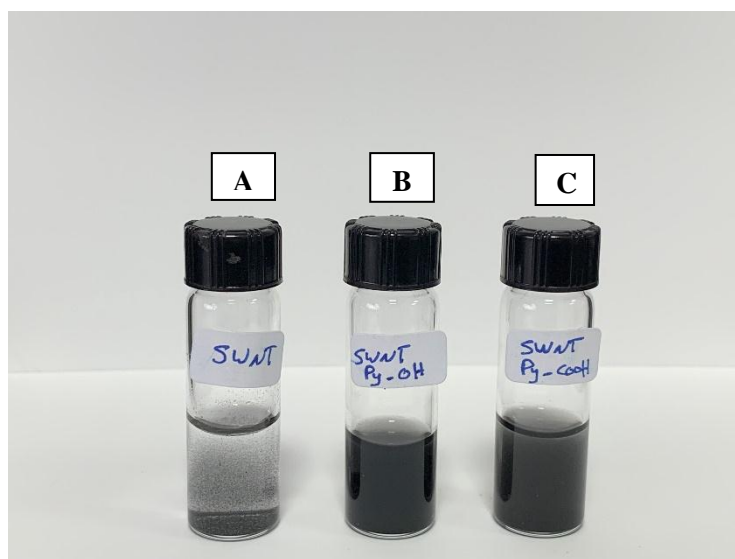


Figure 3.1: Image of dispersion of A) p-SWCNTs; B) SWCNTs-Py-OH and C) SWCNTs-Py-COOH.

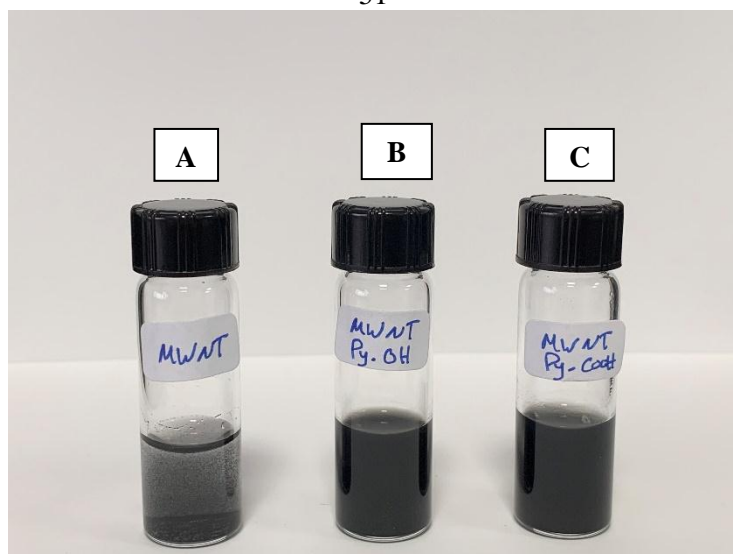


Figure 3.2: Image of dispersion of A) p-MWCNTs; B) MWCNTs-Py-OH and (C) MWCNTs-Py-COOH.

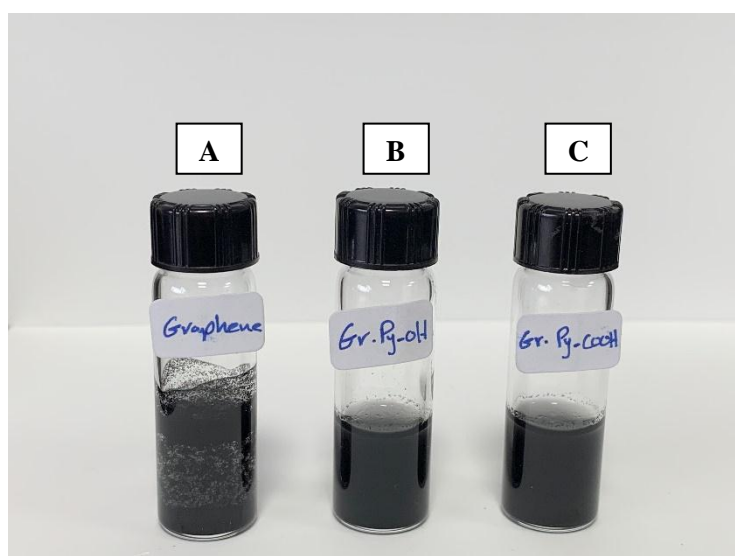


Figure 3.3: Image of dispersion of A) p-graphene; B) Graphene-Py-OH and C) Graphene-Py-COOH.

3.2.2 Size and morphology of carbon nanomaterials

The size and morphology of *f*-SWCNTs, *f*-MWCNTs and *f*-graphene were inspected by TEM images (figure 3.4). These images of *f*-SWCNTs and *f*-MWCNTs elucidate the separation between the nanotubes sidewalls and so

a separated individual nanotube with a diameter in the range of (5-15) nm can be observed. Also, the images of *f*-graphene elucidate the separation between the graphene sheets and so a separated single sheet of graphene can be observed with diameter in the range of (0.6-0.8) μm . Actually, the functionalization of carbon nanomaterials has a de-bundling effect because of the decrease in the hydrophobic interactions between the nanotubes sidewalls of the *f*-SWCNTs and *f*-MWCNTs and the graphene sheets of the *f*-graphene.

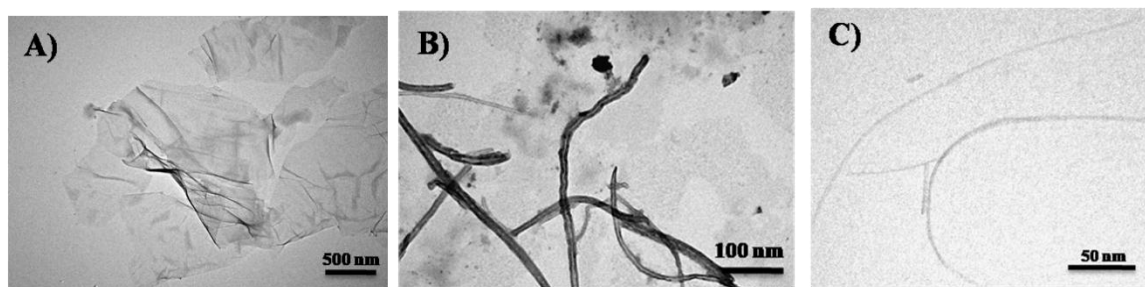


Figure 3.4: TEM images of A) *f*-graphene; B) *f*-MWCNTs and C) *f*-SWCNTs.

3.2.3 UV-vis spectrophotometry

The π - π stacking between the pyrene moieties and the carbon nanostructures was confirmed by absorption spectra. Pyrene has characteristic three peaks at 245, 275 and 345 nm due to the π -conjugation system (109). Upon the incubation with the carbon nanostructures, the three peaks are observed which confirms the presence of pyrene moieties but there is a quenching effect of the absorption due to the interaction with the surface of the carbon nanostructures (110). This confirms the successful π - π stacking between the pyrene moieties and the carbon nanostructures as we can observe in (figure 3.5).

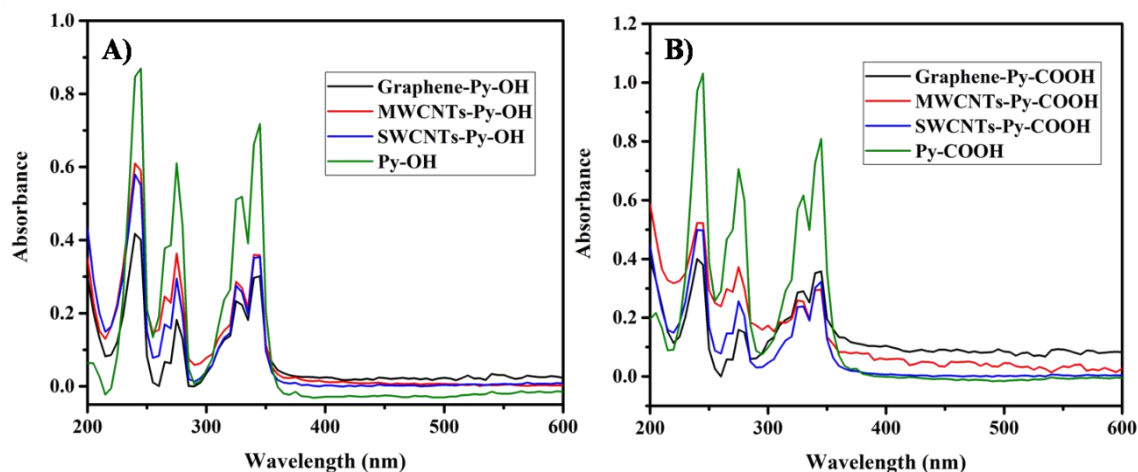


Figure 3.5: UV-Vis spectra of A) Py-OH, Graphene-Py-OH, MWCNTs-Py-OH, SWCNTs-Py-OH and B) Py-COOH, Graphene-Py-COOH, MWCNTs-Py-COOH, SWCNTs-Py-COOH.

3.2.4 Thermogravimetric analysis (TGA)

Thermogravimetric analysis (TGA) was used to quantify the amount of functionalization of the used carbon nanomaterials. As shown in previous studies that the carbon nanomaterials (graphene, MWCNTs, and SWCNTs) are thermostable nanomaterials until 600 degree Celsius ($^{\circ}\text{C}$) and most organic compounds are completely degraded at this high temperature (111). Therefore, upon heating our functionalized carbon nanomaterials, the weight loss in the conjugate will be related to amount of pyrene moieties attached at the surface. In (figure 3.6), it could be observed that the amount of functionalization in all carbon nanomaterials is nearly equal in the range of 17-29%. As the hydrophobic component is the same, therefore there is an almost equal amount of functionalization that sufficient to disperse the carbon nanomaterials perfectly in water as were observed previously in (figures 3.1, 3.2 and 3.3).

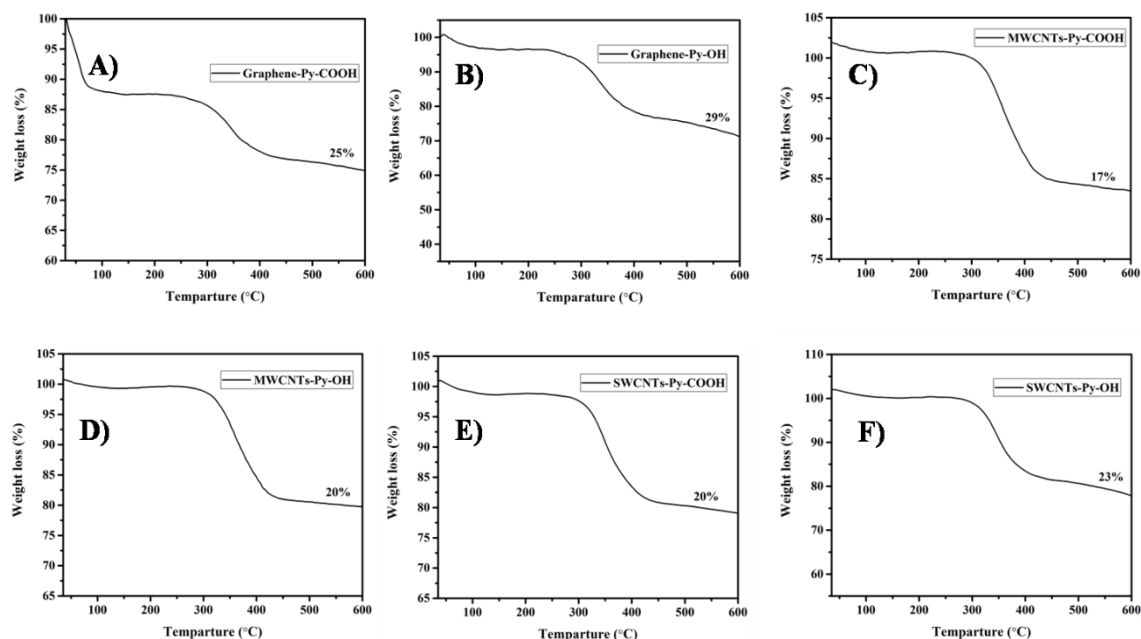


Figure 3.6: Thermogravimetric analysis of all functionalized carbon nanomaterials: A) Graphene-Py-COOH; B) Graphene-Py-OH; C) MWCNTs-Py-COOH; D) MWCNTs-Py-OH; E) SWCNTs-Py-COOH and F) SWCNTs-Py-OH.

3.2.5 Zeta potential

Zeta potential is used to analyze the charge of the outer surface of the nanomaterials. Studies showed that zeta potential value above ± 20 mV indicates the formation of a stable suspension (112). Herein, we measured the zeta potential for all of our functionalized carbon nanostructures (SWCNTs-Py-OH, SWCNTs-Py-COOH, MWCNTs-Py-OH, MWCNTs-Py-COOH, graphene-Py-OH and graphene-Py-COOH) using phase analysis light scattering (PALS) technique (table 1). We obtained in all cases negative values around 20 mV that indicated the formation of a stable suspension and the negative values are due to the presence of hydroxyl and carboxyl groups on the surface of the functionalized carbon nanostructures.

Table 2: Zeta potential values for all of our functionalized carbon nanostructures.

<i>f</i> -carbon nanostructures	Zeta potential (mV)
SWCNTs-Py-OH	-19.41
SWCNTs-Py-COOH	-18.11
MWCNTs-Py-OH	-21.12
MWCNTs-Py-COOH	-20.47
Graphene-Py-OH	-24.84
Graphene-Py-COOH	-19.49

3.3 Connective tissues casting and characterization

3.3.1 3T3 cells-based ECTs

3.3.1.1 Generation of ECTs with 3T3 cells

ECTs containing 3T3 cells were generated with different concentrations of CNTs or graphene (figure 3.7). The control tissues were whitish, opaque, rounded and cohesive disk while the incorporation of CNTs or graphene loading made the tissues appear dark-gray depending on the kind and concentration of CNTs or graphene. There was no contraction in the tissues over 5 days in culture as the tissues were still occupying the whole culture surface of the well in a 48-well-plate therefore we further investigated the viability of the cells by MTS assay in addition to histopathological evaluation and analysis of SEM imaging.

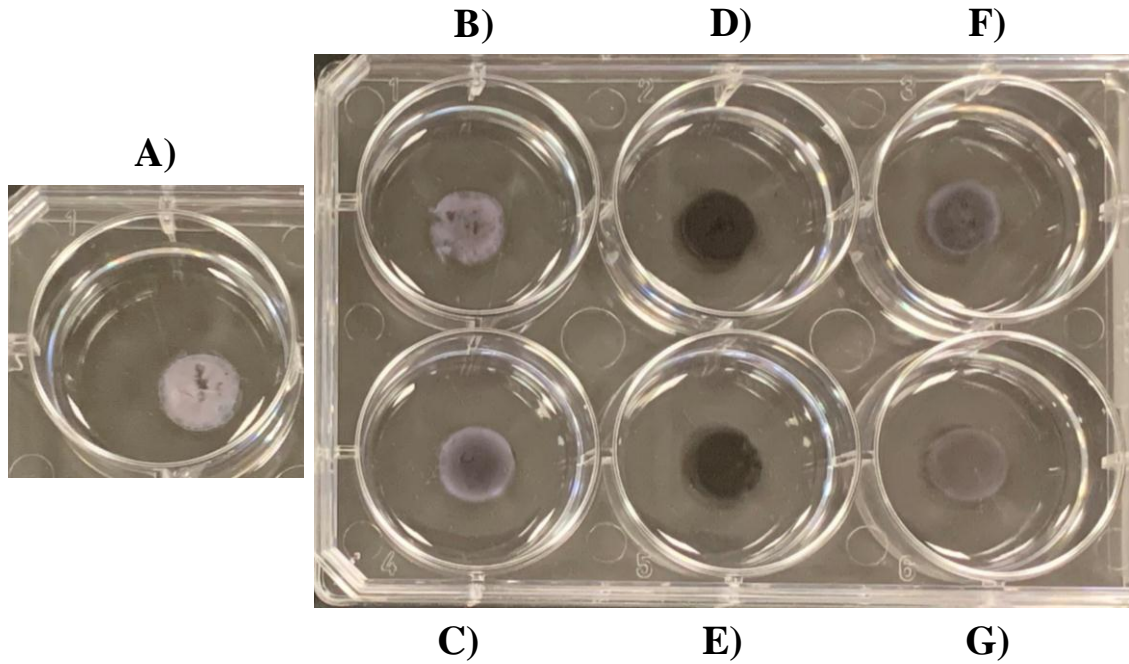


Figure 3.7: Gross examination of 3T3-containing ECT with varying CNTs or graphene loading: A) Control; B) SWCNTs-Py-OH (0.050%); C) SWCNTs-Py-COOH (0.050%); D) MWCNTs-Py-OH (0.050); E) MWCNTs-Py-COOH (0.050%); F) Graphene-Py-OH (0.010%) and G) Graphene-Py-COOH (0.010%).

3.3.1.2 Electrical conductivity of ECTs

The formation of integrated three-dimensional network of all kinds of CNTs or graphene within the collagen matrix was associated with a significant enhancement in the electrical conductivity of the tissues that was mostly kind-dependent (figure 3.8).

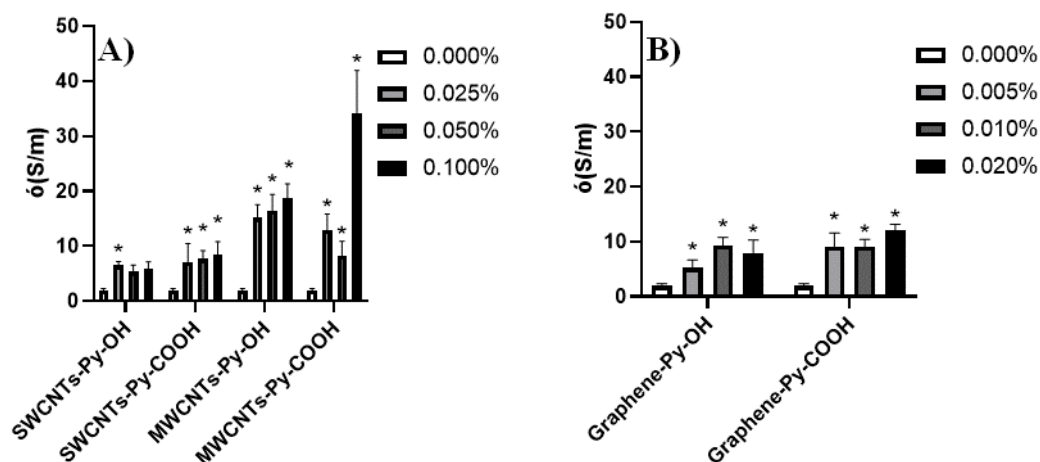


Figure 3.8: Average electrical conductivity of ECT constructs of 3T3 cells with different A) CNTs loading or B) graphene loading. The symbol * indicates significance ($P \leq 0.05$) with respect to control (0.000%). The statistical significance was determined by two-way ANOVA.

The data demonstrated that the enhancement of the conductivity was highest with MWCNTs-Py-COOH, followed by MWCNTs-Py-OH, SWCNTs-Py-COOH and SWCNTs-Py-OH. Therefore, in general MWCNTs species could enhance the conductivity more than SWCNTs species. Also, functionalization of CNTs or graphene with -COOH could result in a greater conductivity compared with functionalization with -OH (figure 3.9). In MWCNTs-Py-OH the conductivity was concentration-dependent. CNTs and graphene are cytotoxic in high concentrations. However, the increase in the conductivity was associated with a reduction in cell viability indicating that the tissue conductivity was most likely dependent on the degree of enrichment by CNTs/graphene, rather than the cell content.

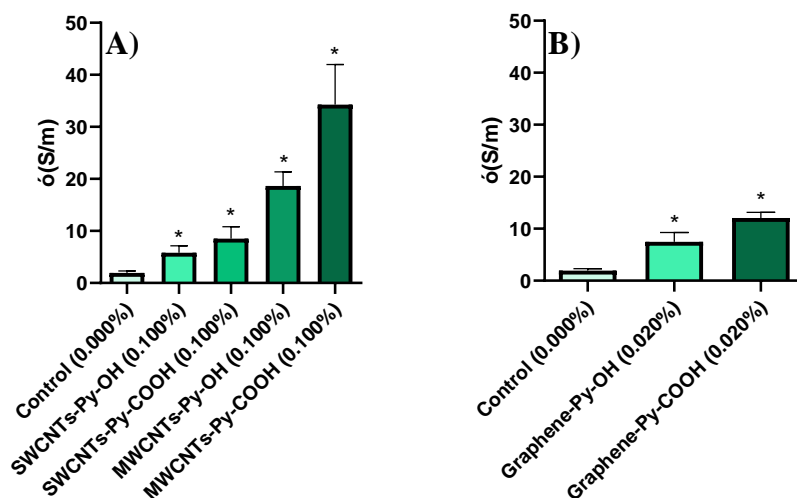


Figure 3.9: Average electrical conductivity of ECT constructs of 3T3 cells with the highest A) CNTs loading or B) graphene loading. The symbol * indicates significance ($P \leq 0.05$) with respect to control. The statistical significance was determined by Student t-test.

3.3.1.3 Cell viability test

Monolayer two-dimensional cultures of 3T3 cells were incubated over 24 hours in culture media containing the different species of CNTs or graphene by using equivalent concentrations to those used in the ECT. The viability of 3T3 cells was investigated by microscopic examination of the cell morphology and by MTS assay. As noticed in (figure 3.10) the control cells and those incubated with 0.025% of different kinds of CNTs or (0.005%) graphene loading appeared normal, spread and well-adhered to the plastic surface. However, with higher CNT or graphene concentrations the cells appeared less spread on the plastic surface and the morphology of some cells was abnormal. Such changes appeared concentration-dependent.

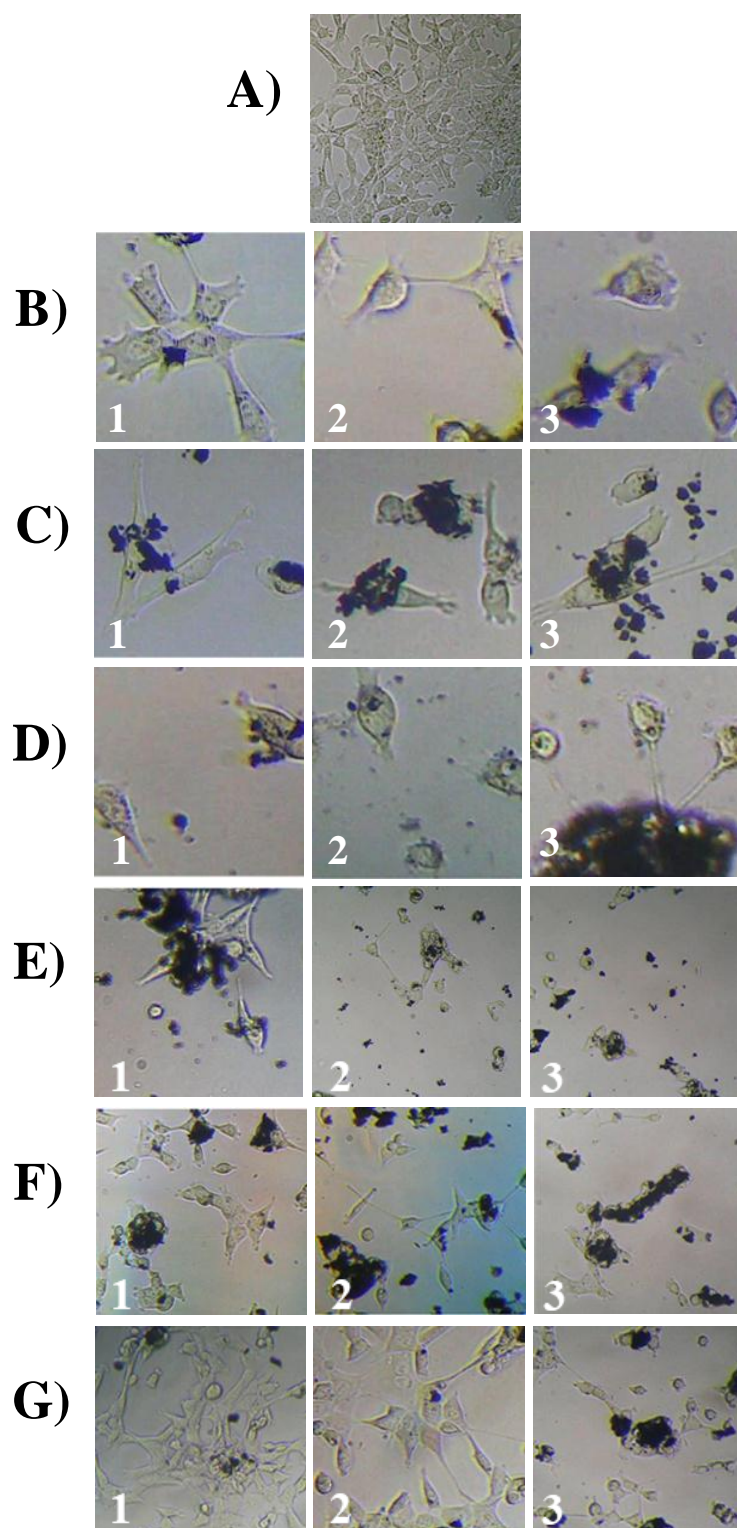


Figure 3.10: Bright field images at 100 \times for 3T3 cells treated with different concentrations of CNTs (0.025%, 0.050% and 0.100%), images 1-3, respectively or graphene (0.005%, 0.010% and 0.020%), images 1-3, respectively after 48 hours : A) Control (3T3 cells without treatment); B) SWCNTs-Py-OH; C) SWCNTs-Py-COOH; D) MWCNTs-Py-OH; E) MWCNTs-Py-COOH; F) Graphene-Py-OH and G) Graphene-Py-COOH.

The data from MTS analysis (figure 3.11) demonstrated that compared to the control cells there were a statistically significant concentration-dependent reduction in 3T3 cells viability. The concentrations 0.025% of CNTs and 0.005% of graphene derivatives reduced the cell viability between around (10-30) %. These concentrations were found in the previous experiments to be enough to significantly enhance the electrical conductivity of the tissues. Therefore, there would be no need to include the higher concentrations in future studies for generating electrically conductive tissues.

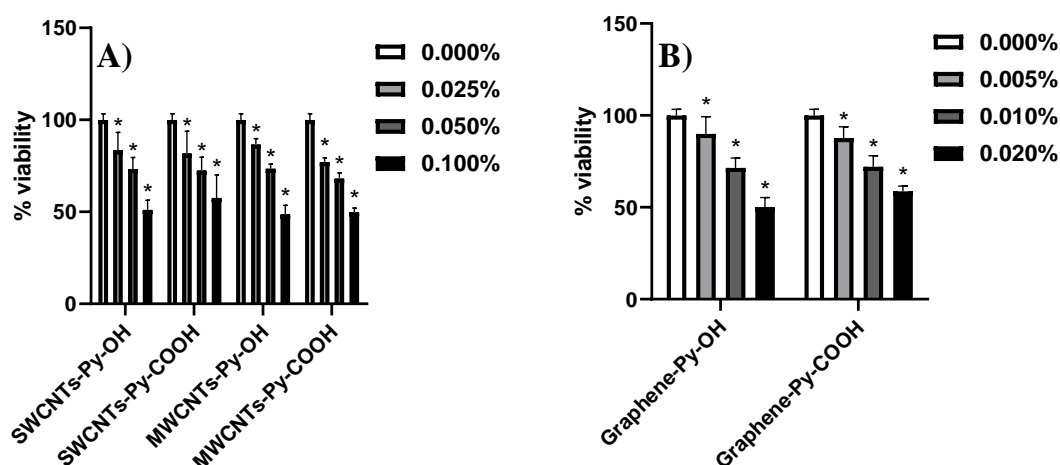


Figure 3.11: Concentration-dependent effect of A) CNTs species or B) graphene species on the viability of 3T3 cells over 24 hours. The symbol * indicates significance ($P \leq 0.05$) with respect to control (0.000%). The statistical significance was determined by two-way ANOVA.

3.3.1.4 Histopathological evaluation for ECTs

H%E stain was utilized to study the organization of ECM, shape and distribution of 3T3 cells and possible interaction of CNTs or graphene with cells while Masson's trichrome stain was utilized to study the level of fibrosis in tissue samples from 3T3 cells-based ECTs (figure 3.12).

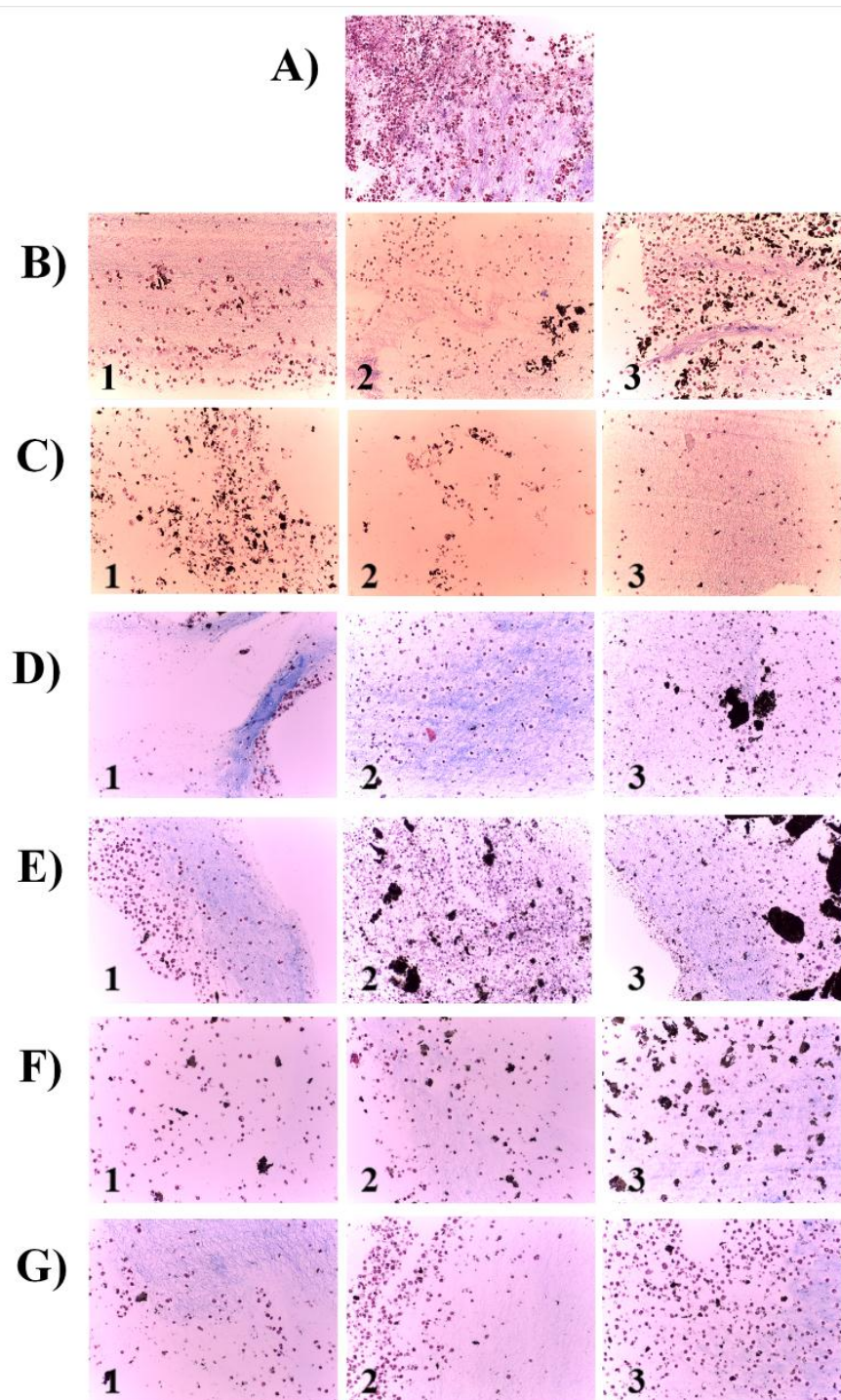


Figure 3.12: Digital microscopic images of ECT constructs stained with Masson's trichrome stain and varying concentrations of CNTs (0.025%, 0.050% and 0.100%), images 1-3, respectively or graphene (0.005%, 0.010% and 0.020%), images 1-3, respectively: A) Control (3T3 cells without treatment); B) SWCNTs-Py-OH; C) SWCNTs-Py-COOH; D) MWCNTs-Py-OH; E) MWCNTs-Py-COOH; F) Graphene-Py-OH and G) Graphene-Py-COOH. Blue stain is for collagen, red/pink is for cellular cytoplasm and black is for CNTs or graphene.

The intensity of fibrosis in random images taken for all ECTs was digitally analyzed by ImageJ[®] software (figure 3.13). All species with all tested concentrations of SWCNTs, MWCNTs and graphene species significantly decreased the degree of tissue fibrosis ($P \leq 0.05$) relative to the control tissues with the exception of 0.02% graphene-Py-COOH which exhibited a degree of fibrosis that was similar to that of the control ECT.

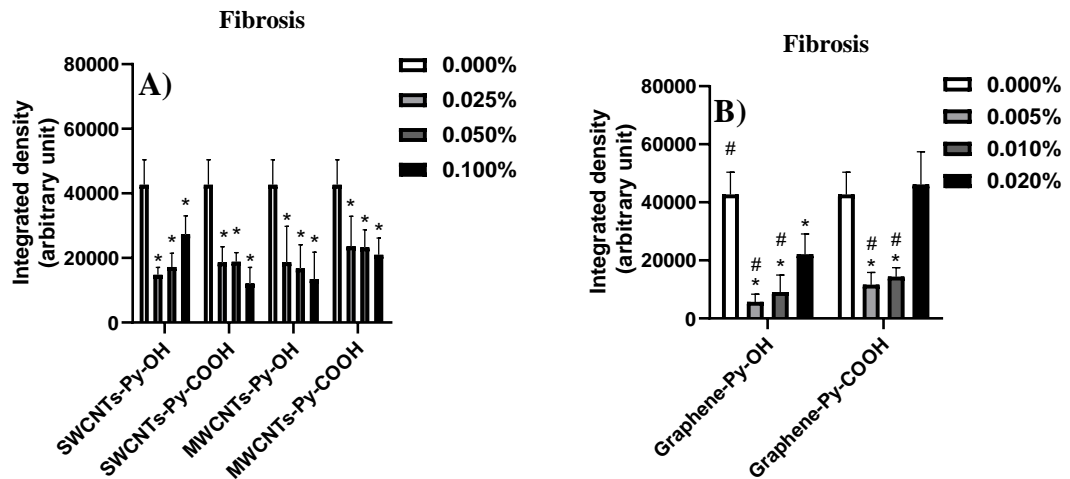


Figure 3.13: Histopathological analysis of ECT constructs of 3T3 cells with different A) CNTs loading or B) graphene loading. The symbols * and # indicate significance ($P \leq 0.05$) with respect to control (0.000%) and the highest graphene loading (0.020%), respectively. The statistical significance was determined by two-way ANOVA. The extent of fibrosis was digitally quantified by the “color deconvolution” plugin in ImageJ.

In agreement, a blinded-histopathological evaluation of the tissues (figure 3.12) demonstrated that the ECM of control ECTs was disorganized indicating that the cells were not able to organize the matrix. This observation is in line with the observation that the ECT did not contract in culture over the 5 days therapy as demonstrated in (figure 3.7). In SWCNTs-Py-OH and SWCNTs-Py-COOH ECTs the ECM was

disorganized at all tested concentrations. The SWCNTs-Py-OH and SWCNTs-Py-COOH particles were randomly dispersed within the ECM but SWCNTs-OH were not observed inside the 3T3 cells so there was no interaction between SWCNTs-Py-OH and these cells in all concentrations. On the other side, in all SWCNTs-Py-COOH samples some particles could be spotted within the cells and this was associated with more cell disruption. In samples containing MWCNTs-Py-OH and MWCNTs-Py-COOH the CNTs particles were dispersed throughout the ECM and also within the cells at all tested concentrations. In the 0.100% and 0.050% concentrations the ECM was highly disorganized while in the 0.025% concentration the ECM was better organized and the cells appeared more intact despite the MWCNTs-Py-OH and MWCNTs-Py-COOH deposition within the cells indicating that this concentration of MWCNTs-Py-OH and MWCNTs-Py-COOH may not be harmful to the cells which is in line with the viability studies by MTS assay mentioned above. Interestingly, SWCNTs-Py-OH and graphene species in general demonstrated a concentration-dependent increase in tissue fibrosis despite of the decrease in the viable 3T3 cells. We assume that this could be due to the induction of collagen deposition by the remaining stressed cells (113). But this needs to be further investigated by future projects.

3.3.1.5 SEM evaluation for ECTs

Detailed SEM imaging of the different kinds of ECTs revealed the formation of distinct patterns of interweaving networks of collagen fibers and CNTs or graphene loading especially in the spaces between the fibers (Figure 3.14). The images were digitally analyzed by ImageJ[®] software to highlight the differences in the microstructures of the tissue matrices as detailed below.

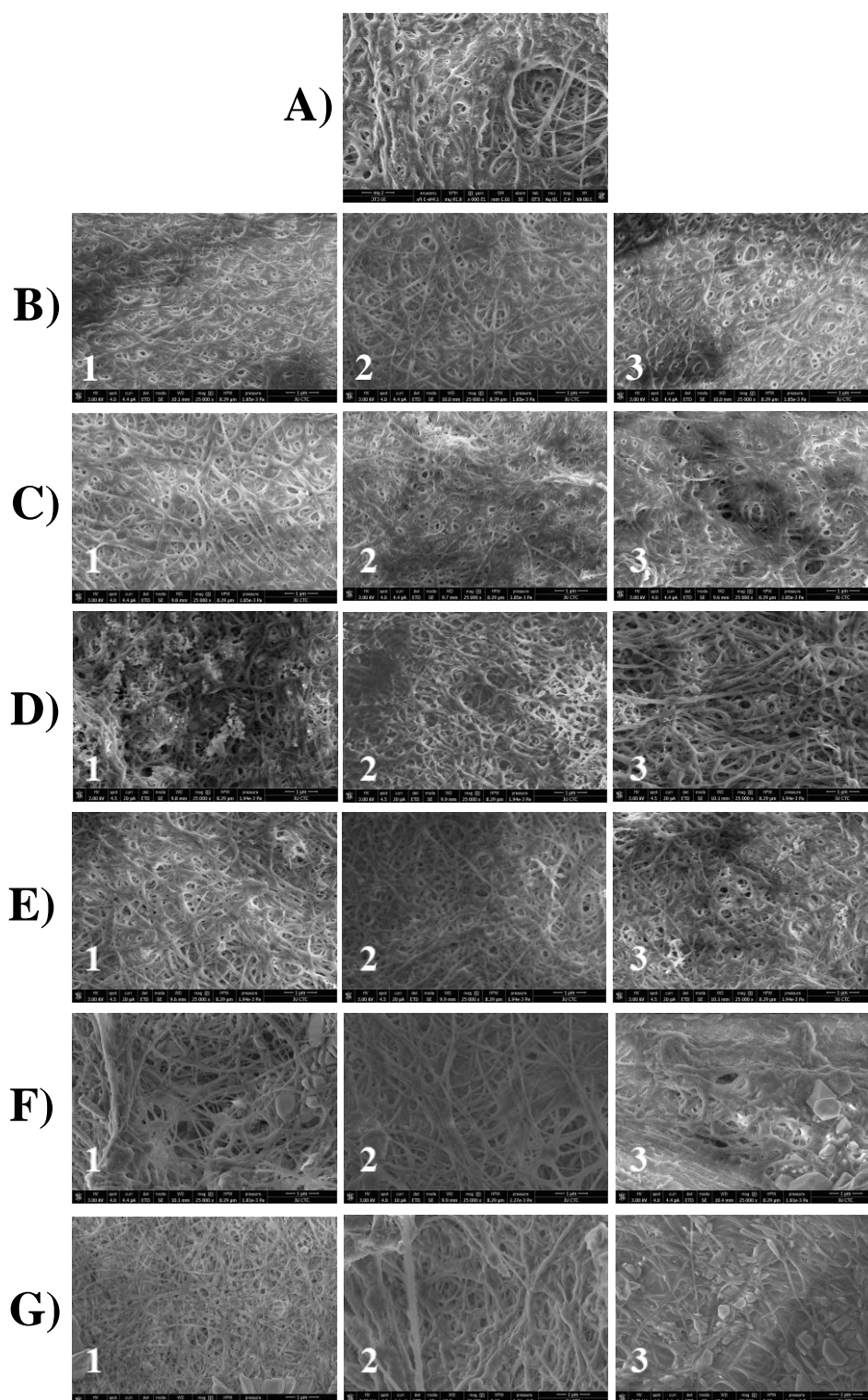


Figure 3.14: SEM images at 5 μm for 3T3 cells treated with different concentrations of CNTs (0.025%, 0.050% and 0.100%), images 1-3, respectively or graphene (0.005%, 0.010% and 0.020%), images 1-3, respectively: A) Control (3T3 cells without treatment); B) SWCNTs-Py-OH; C) SWCNTs-Py-COOH; D) MWCNTs-Py-OH; E) MWCNTs-Py-COOH; F) Graphene-Py-OH and G) Graphene-Py-COOH.

3.3.1.5.1 Analysis of Fiber thickness

Digital analysis of SEM images by ImageJ[®] software demonstrated that the thickness of collagen fibers in all conditions were similar to that of the control with the exception of 0.005% graphene-Py-COOH which exhibited a statistically significant reduction (figure 3.15). Indicating that the inclusion of CNTs or graphene species had no effect on the polymerization of collagen fibers.

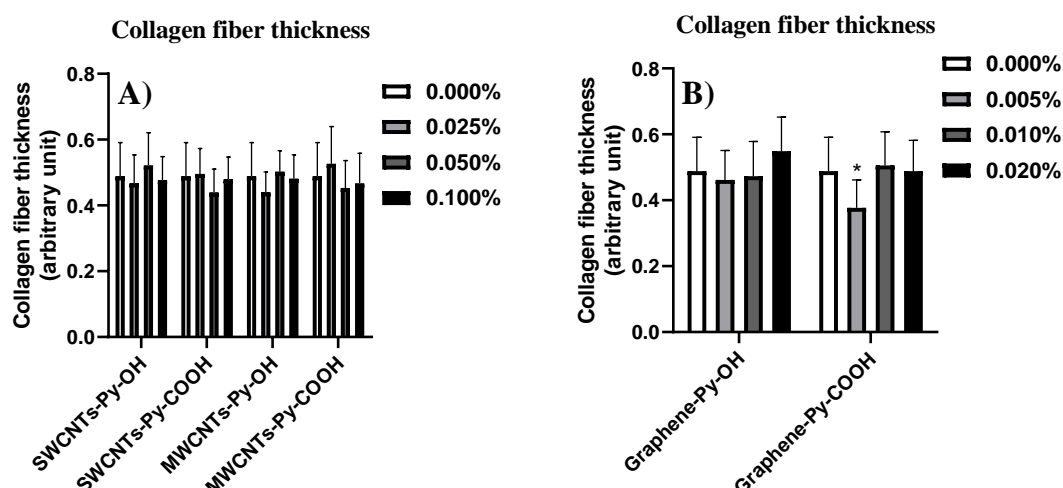


Figure 3.15: SEM evaluation of ECT constructs of 3T3 cells with different A) CNTs loading or B) graphene loading. The symbol * indicates significance ($P \leq 0.05$) with respect to control (0.000%). The statistical significance was determined by two-way ANOVA. Collagen fiber thickness was digitally quantified by ImageJ.

3.3.1.5.2 Analysis of Matrix porosity

The matrix porosity of random images taken for all ECTs were digitally analysis by ImageJ[®] software (figure 3.16). All CNTs-containing ECTs exhibited statistically significantly decreased in matrix porosity relative to the control. Likewise, ECTs containing 0.005% and 0.010% graphene-Py-

OH and 0.005% graphene-Py-COOH exhibited statistically significant decrease construct matrix porosity relative to control. The decrease in matrix porosity could reflect the formation of more compact matrices in the presence of CNTs and graphene which we hypothesize to be an interaction between the collagen fibers on the one side and CNTs or graphene loading on the other side. However, with 0.010% graphene-Py-COOH and 0.020% graphene of both types the porosity was similar to that of the control. The change in tissue porosity should be a subject for future in depth analysis to elucidate its potential effect on the physical properties of the tissues.

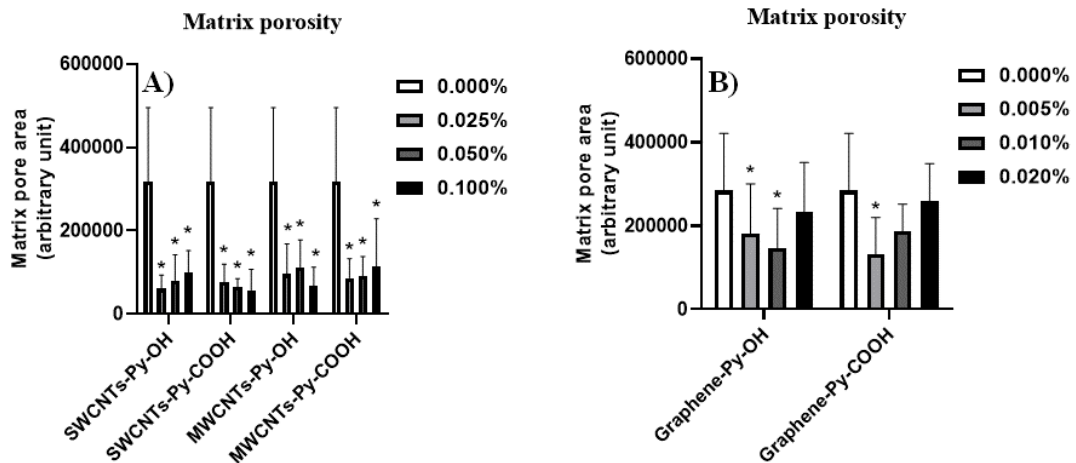


Figure 3.16: SEM evaluation analysis of ECT constructs of 3T3 cells with different A) CNTs loading or B) graphene loading. The symbol * indicates significance ($P \leq 0.05$) with respect to control (0.000%). The statistical significance was determined by two-way ANOVA. Matrix porosity was digitally quantified by ImageJ.

3.3.2 Primary skin fibroblasts-based ECTs

3.3.2.1 Generation of ECTs with Primary skin fibroblast

ECTs containing primary skin fibroblasts were generated with different kinds of CNTs or graphene (figure 3.17). Due to the difficulties in getting a high yield of isolated primary skin fibroblasts some proof of principle experiments were performed by using only one concentration of SWCNTs-Py-OH (0.050%), MWCNTs-Py-OH (0.050%) and graphene-Py-OH (0.010%). The control tissues were opaque, white, rounded and cohesive disk while the incorporation of CNTs or graphene loading caused visible darkening of the rounded cohesive disks. Compared with 3T3 cells-containing ECTs these tissues with primary skin fibroblasts were better in cohesiveness and compaction. They contracted over 5 days in culture and that was assessed by measuring the diameter of the tissues which indicate that these cells can better interact and organize the ECM fibers.

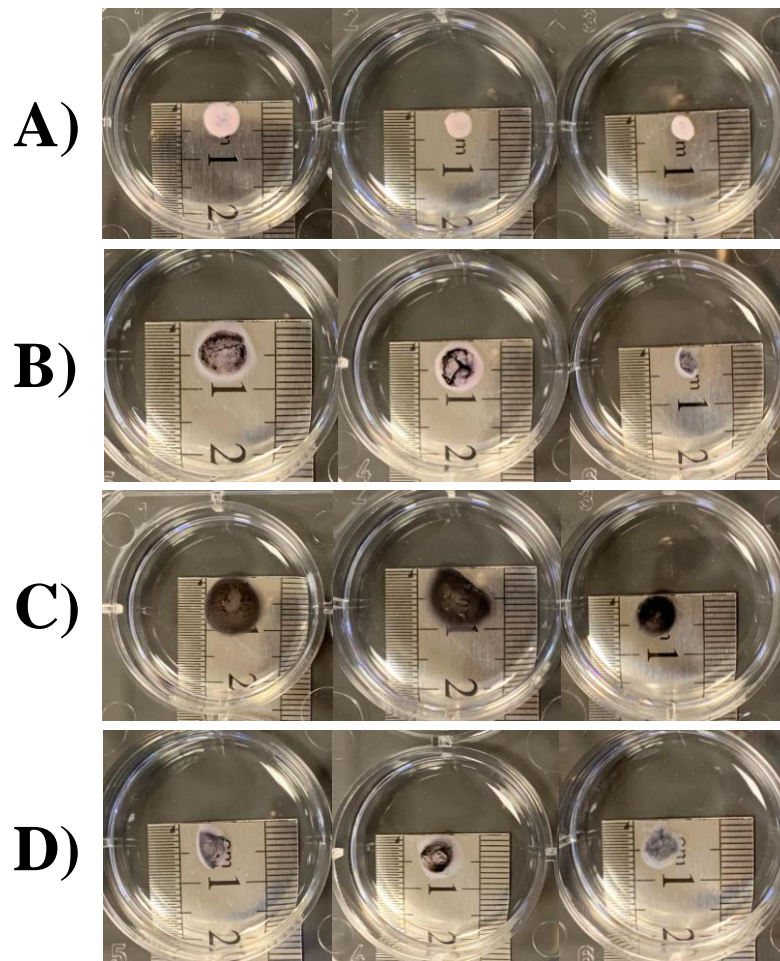


Figure 3.17: Images of ECT constructs contraction with varying CNTs or graphene loading: A) Control (Primary skin fibroblasts); B) SWCNTs-Py-OH (0.050%); C) MWCNTs-Py-OH (0.050%) and D) Graphene-Py-OH (0.010%).

As shown in (figure 3.18) the presence of 0.050% MWCNTs-Py-OH and 0.010% graphene-Py-OH significantly reduced the contraction of the tissues as evidenced by a significant increase in tissue diameter which indicates that these CNTs and graphene species might modulate the interaction of the cells with ECM.

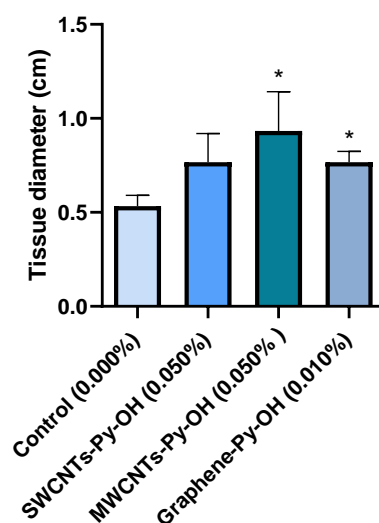


Figure 3.18: The ECT constructs of primary skin fibroblasts with varying CNTs or graphene loading diameter measurements. The symbol * indicates significance ($P \leq 0.05$) with respect to control. The statistical significance was determined by Student t-test.

3.3.2.2 Electrical conductivity of ECTs

As shown in (figure 3.19) MWCNTs and graphene loading significantly increased the electrical conductivity of the ECTs as compared to the control (collagen only ECTs). Moreover, MWCNTs-Py-OH were more efficient in enhancing the electrical conductivity than graphene-Py-OH. SWCNTs-Py-OH did not exhibit any statistically significant enhancement in electrical conductivity of the ECTs as compared to the control. Compared with the 3T3 cells-based ECTs containing corresponding concentrations of CNTs or graphene the conductivity primary skin fibroblasts-based ECTs appears to be lower which could be due to a greater collagen matrix compaction in these ECTs which we hypothesize to negatively influenced the efficient formation of CNTs or graphene networks. Further future studies are required to investigate this hypothesis.

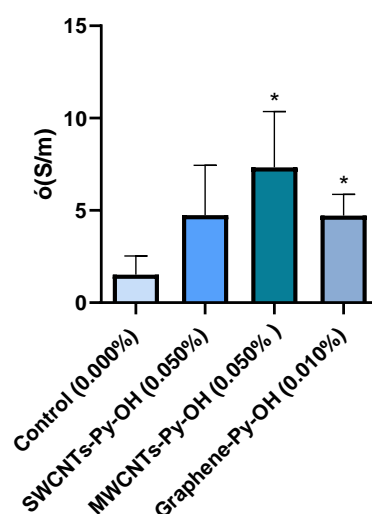


Figure 3.19: Average electrical conductivity of ECT constructs of primary skin fibroblasts with different CNTs loading or graphene loading. The symbol * indicates significance ($P \leq 0.05$) with respect to control. The statistical significance was determined by Student t-test.

3.3.2.3 Histopathological evaluation for ECTs

For a deep insight to the structure and organization of the ECTs again the H%E stain was utilized to study the organization of ECM content, shape and distribution of primary skin fibroblasts and possible interaction of CNTs or graphene with cells while Masson's trichrome stain was used to study the degree of fibrosis in tissue samples (figure 3.20).

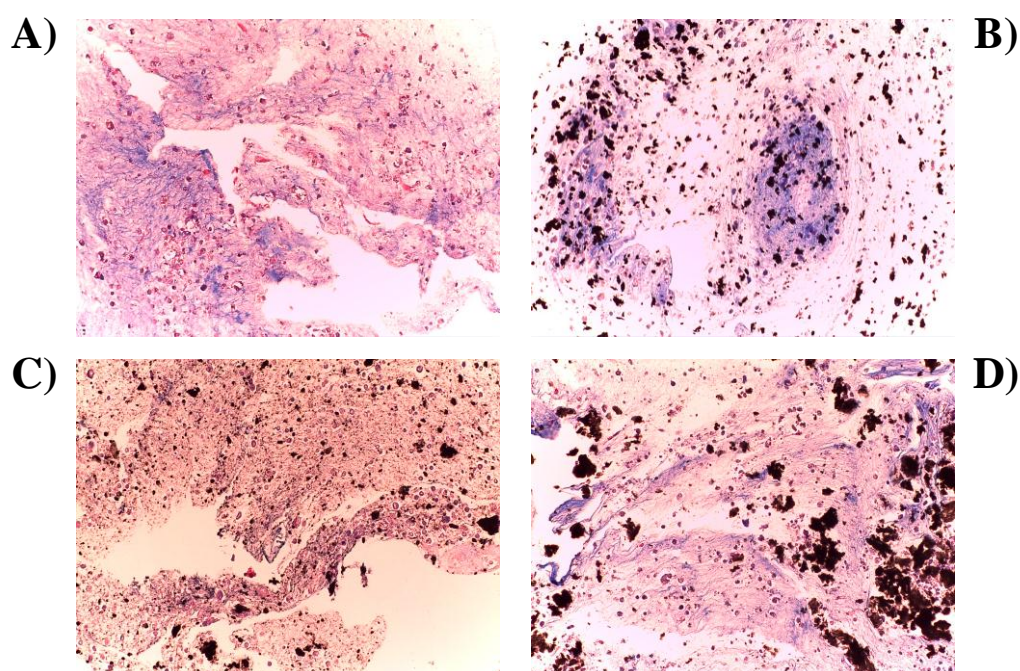


Figure 3.20: Digital microscopic images of ECT constructs stained with Masson's trichrome stain and varying CNTs or graphene loading: A) Control (Primary skin fibroblasts); B) SWCNTs-Py-OH (0.050%); C) MWCNTs-Py-OH (0.050%) and D) Graphene-Py-OH (0.010%). Blue stain is for collagen, red/pink is for cellular cytoplasm and black is for CNTs or graphene.

The intensity of fibrosis in random images taken for all ECTs was digitally analyzed by ImageJ[®] software (figure 3.21). The presence of 0.050% MWCNTs-Py-OH exhibited a statistically significantly decrease in the degree of fibrosis ($P \leq 0.05$) while SWCNTs-Py-OH (0.050%) and graphene-Py-OH (0.010%) did not show any effect.

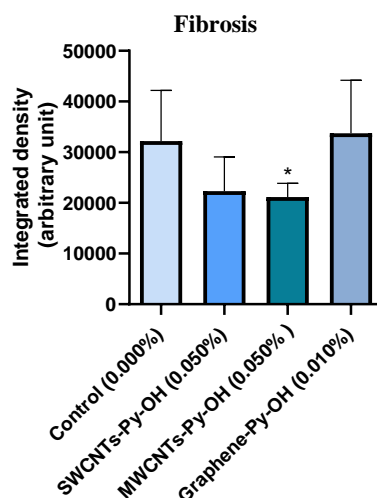


Figure 3.21: Histopathological analysis of ECT constructs of primary skin fibroblasts with different CNTs loading or graphene loading. The symbol * indicates significance ($P \leq 0.05$) with respect to control (0.000%). The statistical significance was determined by Student t-test. The extent of fibrosis was digitally quantified by the “color deconvolution” plugin in ImageJ.

The histopathological evaluation revealed that ECM of control was normally organized and the primary skin fibroblasts appeared normal and healthy (figure 3.20). In SWCNTs-Py-OH (0.050%) and graphene-Py-OH (0.010%) samples the status of the ECM and the fibroblasts were similar to that of the control with SWCNTs-Py-OH or graphene-Py-OH dispersed throughout the ECM but not inside the fibroblasts indicating that there could be no significant interaction between fibroblasts and SWCNTs-Py-OH or graphene-Py-OH which might explain the relatively low effect on the tissue fibrosis as shown earlier (figure 3.21). However, in samples of MWCNTs-Py-OH (0.050%) the ECM was relatively disorganized and there were some disrupted fibroblasts and some MWCNTs-Py-OH particles deposited inside them which might explain the reduction in tissue fibrosis observed before (figure 3.21).

3.3.2.4 SEM evaluation for ECTs

Scanning electron microscopy utilized to study the microstructure of the different ECT matrices that are based on the primary skin fibroblasts demonstrated some differences in the pattern and morphology of the fibers that compose the matrices (Figure 3.22). The collagen fibers in the control matrix were very well defined and distinct while in the other conditions; the collagen fibers were highly compacted and poorly defined.

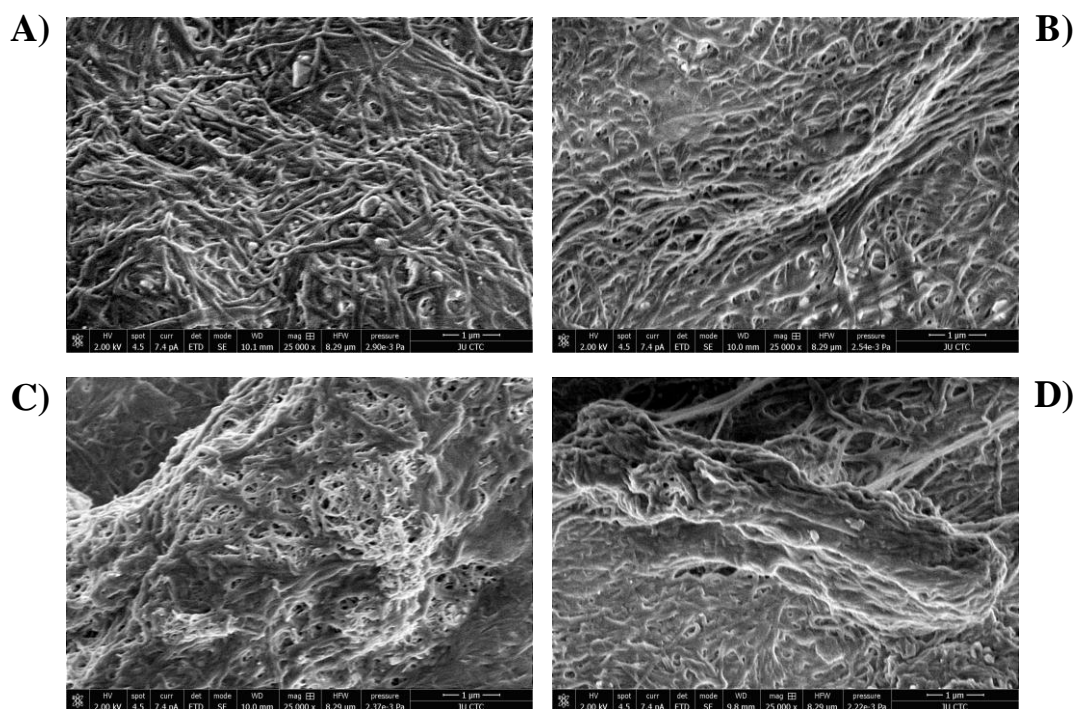


Figure 3.22: SEM images at 5 µm for varying CNTs or graphene loading: A) Control (Primary skin fibroblasts); B) SWCNTs-Py-OH (0.050%); C) MWCNTs-Py-OH (0.050%) and D) Graphene-Py-OH (0.010%).

3.3.2.4.1 Analysis of Fiber thickness

The collagen fiber thickness of random images taken for all ECT constructs were digitally analysis by ImageJ[®] software (figure 3.23). All ECTs of CNTs and graphene loading did not exhibit any statistically significant change on collagen fiber thickness relative to the control indicating no effects of collagen fiber polymerization and deposition.

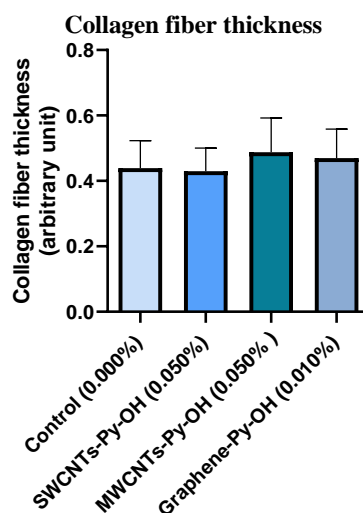


Figure 3.23: SEM evaluation of ECT constructs of primary skin fibroblasts with different CNTs loading or graphene loading. There is no significance ($P \leq 0.05$) with respect to control (0.000%). The statistical significance was determined by Student t-test. Collagen fiber thickness was digitally quantified by the “color deconvolution” plugin in ImageJ.

3.3.2.4.2 Analysis of Matrix porosity

The matrix porosity of random images taken for all ECT constructs were digitally analysis by ImageJ[®] software (figure 3.24). ECTs of 0.050% SWCNTs loading exhibited statistically significant decrease in construct matrix porosity relative to the control. The porosity of the ECTs containing

MWCNTs or graphene loading exhibited similar porosity to that of the control ECTs. By taken together with the conductivity data (figure 3.19) it can be assumed that the porosity of the ECT does not correlate with the conductivity of the tissue.

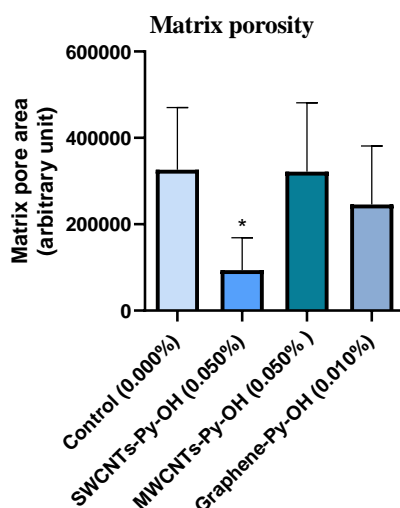


Figure 3.24: SEM evaluation of ECT constructs of primary skin fibroblasts with different CNTs loading or graphene loading. The symbol * indicates significance ($P \leq 0.05$) with respect to control (0.000%). The statistical significance was determined by Student t-test. Matrix porosity was digitally quantified by the “color deconvolution” plugin in ImageJ.

Conclusion

Effective noncovalent functionalization of CNTs and graphene has been achieved. This functionalization shown a good dispersibility as approved by TEM. The successful π - π stacking between the pyrene moieties and the carbon nanostructures was confirmed by absorption spectra and the degree of functionalization was nearly equal in the range of 17-29% in all carbon nanomaterials. Moreover, the zeta potential data showed around -20 mV in all cases that indicated the formation of a stable suspension. ECT constructs containing 3T3 cells have shown a significant enhancement in the electrical conductivity of the tissues and that was mostly kind-dependent. The data demonstrated that in general MWCNTs species could enhance the conductivity more than SWCNTs species. Also, functionalization of CNTs or graphene with $-\text{COOH}$ could result in a greater conductivity compared with functionalization with $-\text{OH}$. In MWCNTs-Py-OH the conductivity was concentration-dependent. The increase in the conductivity was associated with a reduction in cell viability indicating that the tissue conductivity was most likely dependent on the degree of enrichment by CNTs/graphene, rather than the cell content. Moreover, the intensity of fibrosis was enhanced in comparison to the control tissue. In samples containing (0.025%) MWCNTs-Py-OH and MWCNTs-Py-COOH the ECM was better organized and the cells appeared more intact despite the MWCNTs-Py-OH and MWCNTs-Py-COOH deposition within the cells indicating that this concentration of MWCNTs-Py-OH and MWCNTs-Py-COOH may not be harmful to the cells which is

in line with the viability studies by MTS assay. According to matrix porosity all CNTs-containing ECTs exhibited statistically significantly decreased in matrix porosity relative to the control. The decrease in matrix porosity could reflect the formation of more compact matrices in the presence of CNTs which we hypothesize to be an interaction between the collagen fibers on the one side and CNTs loading on the other side. The change in tissue porosity should be a subject for future in depth analysis to elucidate its potential effect on the physical properties of the tissues. Taken together, the developed constructs showed a great potential for further in vivo studies as engineered tissue.

References

1. Hirsch A. **The era of carbon allotropes.** Nature Materials. 2010;9(11):868-71.
2. Manawi Y, Ihsanullah, Samara A, Al-Ansari T, Atieh M. **A Review of Carbon Nanomaterials' Synthesis via the Chemical Vapor Deposition (CVD) Method.** Materials. 2018;11(5).
3. Katsnelson MI. **Graphene: carbon in two dimensions.** Materials Today. 2007;10(1-2):20-7.
4. Nardecchia S, Carriazo D, Ferrer ML, Gutiérrez MC, del Monte F. **Three dimensional macroporous architectures and aerogels built of carbon nanotubes and/or graphene: synthesis and applications.** Chem Soc Rev. 2013;42(2):794-830.
5. Wu H-C, Chang X, Liu L, Zhao F, Zhao Y. **Chemistry of carbon nanotubes in biomedical applications.** J Mater Chem. 2010;20(6):1036-52.
6. Hu C, Hu S. **Carbon Nanotube-Based Electrochemical Sensors: Principles and Applications in Biomedical Systems.** Journal of Sensors. 2009;2009:1-40.
7. Wilder JWG, Venema LC, Rinzler AG, Smalley RE, Dekker C. **Electronic structure of atomically resolved carbon nanotubes.** Nature. 1998;391(6662):59-62.

8. Mehra N, Jain N. **Drug Delivery Aspects of Carbon Nanotubes.** 2015;628-49.
9. Siegal MP, Overmyer DL, Provencio PP. **Precise control of multiwall carbon nanotube diameters using thermal chemical vapor deposition.** Applied Physics Letters. 2002;80(12):2171-3.
10. Khalid M, Ratnam CT, Walvekar R, Ketabchi MR, Hoque ME. **Reinforced Natural Rubber Nanocomposites: Next Generation Advanced Material.** Green Biocomposites. Green Energy and Technology 2017. p. 309-45.
11. Kunzmann A, Andersson B, Thurnherr T, Krug H, Scheynius A, Fadeel B. **Toxicology of engineered nanomaterials: Focus on biocompatibility, biodistribution and biodegradation.** Biochimica et Biophysica Acta (BBA) - General Subjects. 2011;1810(3):361-73.
12. Vidu R, Rahman M, Mahmoudi M, Enachescu M, Poteca TD, Opris I. **Nanostructures: a platform for brain repair and augmentation.** Frontiers in Systems Neuroscience. 2014;8.
13. Hopley EL, Salmasi S, Kalaskar DM, Seifalian AM. **Carbon nanotubes leading the way forward in new generation 3D tissue engineering.** Biotechnology Advances. 2014;32(5):1000-14.
14. Tasis D, Tagmatarchis N, Bianco A, Prato M. **Chemistry of Carbon Nanotubes.** Chemical Reviews. 2006;106(3):1105-36.

15. Alshehri R, Ilyas AM, Hasan A, Arnaout A, Ahmed F, Memic A. ***Carbon Nanotubes in Biomedical Applications: Factors, Mechanisms, and Remedies of Toxicity.*** *Journal of Medicinal Chemistry.* 2016;59(18):8149-67.
16. Harrison BS, Atala A. **Carbon nanotube applications for tissue engineering.** *Biomaterials.* 2007;28(2):344-53.
17. Hamzah AA, Selvarajan RS, Majlis BY. **Graphene for Biomedical Applications: A Review.** *Sains Malaysiana.* 2017;46 (7):1125-39.
18. Singh V, Joung D, Zhai L, Das S, Khondaker SI, Seal S. **Graphene based materials: Past, present and future.** *Progress in Materials Science.* 2011;56(8):1178-271.
19. Berry V. **Impermeability of graphene and its applications.** *Carbon.* 2013;62:1-10.
20. Hwang J, Yoon T, Jin SH, Lee J, Kim T-S, Hong SH, et al. **Enhanced Mechanical Properties of Graphene/Copper Nanocomposites Using a Molecular-Level Mixing Process.** *Advanced Materials.* 2013;25(46):6724-9.
21. Tan YB, Lee J-M. **Graphene for supercapacitor applications.** *Journal of Materials Chemistry A.* 2013;1(47).

22. Goenka S, Sant V, Sant S. ***Graphene-based nanomaterials for drug delivery and tissue engineering***. **Journal of Controlled Release**. 2014;173:75-88.
23. Liu Z, Tabakman SM, Chen Z, Dai H. **Preparation of carbon nanotube bioconjugates for biomedical applications**. **Nature Protocols**. 2009;4(9):1372-81.
24. Kuila T, Bose S, Mishra AK, Khanra P, Kim NH, Lee JH. **Chemical functionalization of graphene and its applications**. **Progress in Materials Science**. 2012;57(7):1061-105.
25. Lei J, Ju H. **Nanotubes in biosensing**. **Wiley Interdisciplinary Reviews: Nanomedicine and Nanobiotechnology**. 2010;2(5):496-509.
26. Assali M, Leal MP, Fernández I, Romero-Gomez P, Baati R, Khier N. **Improved non-covalent biofunctionalization of multi-walled carbon nanotubes using carbohydrate amphiphiles with a butterfly-like polyaromatic tail**. **Nano Research**. 2010;3(11):764-78.
27. Dresselhaus MS, Dresselhaus G, Avouris P. **Carbon Nanotubes 2001**.
28. Holzinger M, Vostrowsky O, Hirsch A, Hennrich F, Kappes M, Weiss R, et al. **Sidewall Functionalization of Carbon Nanotubes This work was supported by the European Union under the 5th Framework Research Training Network 1999, HPRNT 1999-00011 FUNCARS**. **Angew Chem Int Ed Engl**. 2001;40(21):4002-5.

29. Bahr JL, Yang J, Kosynkin DV, Bronikowski MJ, Smalley RE, Tour JM. *Functionalization of Carbon Nanotubes by Electrochemical Reduction of Aryl Diazonium Salts: A Bucky Paper Electrode*. **Journal of the American Chemical Society**. 2001;123(27):6536-42.
30. Alonso-Lomillo MA, Rüdiger O, Maroto-Valiente A, Velez M, Rodríguez-Ramos I, Muñoz FJ, et al. **Hydrogenase-Coated Carbon Nanotubes for Efficient H₂Oxidation**. **Nano Letters**. 2007;7(6):1603-8.
31. Loh KP, Bao Q, Ang PK, Yang J. *The chemistry of graphene*. **Journal of Materials Chemistry**. 2010;20(12).
32. Niyogi S, Bekyarova E, Itkis ME, McWilliams JL, Hamon MA, Haddon RC. *Solution Properties of Graphite and Graphene*. **Journal of the American Chemical Society**. 2006;128(24):7720-1.
33. Lomeda JR, Doyle CD, Kosynkin DV, Hwang W-F, Tour JM. *Diazonium Functionalization of Surfactant-Wrapped Chemically Converted Graphene Sheets*. **Journal of the American Chemical Society**. 2008;130(48):16201-6.
34. Zhang C, Tjiu WW, Fan W, Huang S, Liu T. *A novel approach for transferring water-dispersible graphene nanosheets into organic media*. **Journal of Materials Chemistry**. 2012;22(23).

35. Stine R, Ciszek JW, Barlow DE, Lee W-K, Robinson JT, Sheehan PE. **High-Density Amine-Terminated Monolayers Formed on Fluorinated CVD-Grown Graphene.** *Langmuir*. 2012;28(21):7957-61.
36. Chen RJ, Zhang Y, Wang D, Dai H. *Noncovalent Sidewall Functionalization of Single-Walled Carbon Nanotubes for Protein Immobilization.* *Journal of the American Chemical Society*. 2001;123(16):3838-9.
37. Stankovich S, Piner RD, Chen X, Wu N, Nguyen ST, Ruoff RS. *Stable aqueous dispersions of graphitic nanoplatelets via the reduction of exfoliated graphite oxide in the presence of poly(sodium 4-styrenesulfonate).* *J Mater Chem*. 2006;16(2):155-8.
38. Xu Y, Bai H, Lu G, Li C, Shi G. *Flexible Graphene Films via the Filtration of Water-Soluble Noncovalent Functionalized Graphene Sheets.* *Journal of the American Chemical Society*. 2008;130(18):5856-7.
39. Xu H, Zeiger BW, Suslick KS. **Sonochemical synthesis of nanomaterials.** *Chem Soc Rev*. 2013;42(7):2555-67.
40. Byrne MT, Gun'ko YK. **Recent Advances in Research on Carbon Nanotube-Polymer Composites.** *Advanced Materials*. 2010;22(15):1672-88.

41. Liu Z, Tabakman S, Welsher K, Dai H. **Carbon nanotubes in biology and medicine: In vitro and in vivo detection, imaging and drug delivery.** Nano Research. 2010;2(2):85-120.
42. Resende R, Tonelli FMP, Santos AK, Gomes KN, Lorençon E, Ladeira LO, et al. *Carbon nanotube interaction with extracellular matrix proteins producing scaffolds for tissue engineering.* International Journal of Nanomedicine. 2012;4511.
43. Engel E, Michiardi A, Navarro M, Lacroix D, Planell JA. **Nanotechnology in regenerative medicine: the materials side.** Trends in Biotechnology. 2008;26(1):39-47.
44. Williams JK, Andersson K-E. **Regenerative pharmacology: recent developments and future perspectives.** Regenerative Medicine. 2016;11(8):859-70.
45. Petit-Zeman S. **Regenerative medicine.** Nature Biotechnology. 2001;19(3):201-6.
46. Christ GJ, Saul JM, Furth ME, Andersson K-E, Nader MA. **The Pharmacology of Regenerative Medicine.** Pharmacological Reviews. 2013;65(3):1091-133.
47. Pavyde E, Usas A, Maciulaitis R. **Regenerative pharmacology for the treatment of acute kidney injury: Skeletal muscle stem/progenitor cells for renal regeneration?** Pharmacological Research. 2016;113:802-7.

48. Andersson KE, Christ GJ. **Regenerative Pharmacology: The Future Is Now.** *Molecular Interventions.* 2007;7(2):79-86.
49. Schuh A, Kroh A, Korschalla S, Liehn EA, Sobota RM, Biessen EAL, et al. ***Myocardial regeneration by transplantation of modified endothelial progenitor cells expressing SDF-1 in a rat model.*** *Journal of Cellular and Molecular Medicine.* 2012;16(10):2311-20.
50. Schuh A, Korschalla S, Kroh A, Schober A, Marx N, Sonmez T, et al. **Effect of SDF-1 α on Endogenous Mobilized and Transplanted Stem Cells in Regeneration after Myocardial Infarction.** *Current Pharmaceutical Design.* 2014;20(12):1964-70.
51. Song M, Jang H, Lee J, Kim JH, Kim SH, Sun K, et al. **Regeneration of chronic myocardial infarction by injectable hydrogels containing stem cell homing factor SDF-1 and angiogenic peptide Ac-SDKP.** *Biomaterials.* 2014;35(8):2436-45.
52. Resende R, Tonelli FMP, Santos AK, Gomes KN, Lorençon E, Ladeira LO, et al. ***Carbon nanotube interaction with extracellular matrix proteins producing scaffolds for tissue engineering.*** *International Journal of Nanomedicine.* 2012.
53. Atala A. **Recent developments in tissue engineering and regenerative medicine.** *Current Opinion in Pediatrics.* 2006;18(2):167-71.

54. Dahms, Piechota, Dahiya, Lue, Tanagho. *Composition and biomechanical properties of the bladder acellular matrix graft: comparative analysis in rat, pig and human*. British Journal of Urology. 1998;82(3):411-9.
55. Yoo JJ, Meng J, Oberpenning F, Atala A. **Bladder augmentation using allogenic bladder submucosa seeded with cells**. Urology. 1998;51(2):221-5.
56. Adamowicz J, Kowalczyk T, Drewa T. *Tissue engineering of urinary bladder - current state of art and future perspectives*. Cent European J Urol. 2013;66(2):202-6.
57. Jungebluth P, Moll G, Baiguera S, Macchiarini P. **Tissue-Engineered Airway: A Regenerative Solution**. Clinical Pharmacology & Therapeutics. 2011;91(1):81-93.
58. Sikavitsas VI, Bancroft GN, Mikos AG. *Formation of three-dimensional cell/polymer constructs for bone tissue engineering in a spinner flask and a rotating wall vessel bioreactor*. Journal of Biomedical Materials Research. 2002;62(1):136-48.
59. Frantz C, Stewart KM, Weaver VM. *The extracellular matrix at a glance*. Journal of Cell Science. 2010;123(24):4195-200.

60. Guan S, Zhang X-L, Lin X-M, Liu T-Q, Ma X-H, Cui Z-F. *Chitosan/gelatin porous scaffolds containing hyaluronic acid and heparan sulfate for neural tissue engineering*. **Journal of Biomaterials Science, Polymer Edition**. 2012;24(8):999-1014.
61. Murphy AR, Laslett A, O'Brien CM, Cameron NR. **Scaffolds for 3D in vitro culture of neural lineage cells**. *Acta Biomaterialia*. 2017;54:1-20.
62. Carlson BM. **Tissues**. The Human Body 2019. p. 27-63.
63. Woodard HQ, White DR. *The composition of body tissues*. **The British Journal of Radiology**. 1986;59(708):1209-18.
64. Connective Tissues: **Matrix Composition and Its Relevance to Physical Therapy**. Physical Therapy. 1999.
65. Yang G, Rothrauff BB, Tuan RS. **Tendon and ligament regeneration and repair: Clinical relevance and developmental paradigm**. *Birth Defects Research Part C: Embryo Today: Reviews*. 2013;99(3):203-22.
66. Sahoo S, Lok Toh S, Hong Goh JC. *PLGA nanofiber-coated silk microfibrinous scaffold for connective tissue engineering*. **Journal of Biomedical Materials Research Part B: Applied Biomaterials**. 2010;95B(1):19-28.
67. Hasan A, Paul A, Vrana NE, Zhao X, Memic A, Hwang Y-S, et al. **Microfluidic techniques for development of 3D vascularized tissue**. *Biomaterials*. 2014;35(26):7308-25.

68. Hasan A, Ragaert K, Swieszkowski W, Selimović Š, Paul A, Camci-Unal G, et al. ***Biomechanical properties of native and tissue engineered heart valve constructs***. **Journal of Biomechanics**. 2014;47(9):1949-63.
69. Geetha Bai R, Muthoosamy K, Manickam S, Hilal-Alnaqbi A. ***Graphene-based 3D scaffolds in tissue engineering: fabrication, applications, and future scope in liver tissue engineering***. **International Journal of Nanomedicine**. 2019;Volume 14:5753-83.
70. Wong EW, Sheehan PE, Lieber CM. **Nanobeam Mechanics: Elasticity, Strength, and Toughness of Nanorods and Nanotubes**. **Science**. 1997;277(5334):1971-5.
71. Esteves IAAC, Cruz FJAL, Müller EA, Agnihotri S, Mota JPB. **Determination of the surface area and porosity of carbon nanotube bundles from a Langmuirian analysis of sub- and supercritical adsorption data**. **Carbon**. 2009;47(4):948-56.
72. Shin SR, Shin C, Memic A, Shadmehr S, Miscuglio M, Jung HY, et al. **Aligned Carbon Nanotube-Based Flexible Gel Substrates for Engineering Biohybrid Tissue Actuators**. **Advanced Functional Materials**. 2015;25(28):4486-95.

73. Gorain B, Choudhury H, Pandey M, Kesharwani P, Abeer MM, Tekade RK, et al. **Carbon nanotube scaffolds as emerging nanoplatform for myocardial tissue regeneration: A review of recent developments and therapeutic implications.** Biomedicine & Pharmacotherapy. 2018;104:496-508.
74. Haraguchi Y, Shimizu T, Yamato M, Okano T. **Concise Review: Cell Therapy and Tissue Engineering for Cardiovascular Disease.** STEM CELLS Translational Medicine. 2012;1(2):136-41.
75. Opie SR, Dib N. **Surgical and catheter delivery of autologous myoblasts in patients with congestive heart failure.** Nature Clinical Practice Cardiovascular Medicine. 2006;3(S1):S42-S5.
76. Alaiti MA, Ishikawa M, Costa MA. **Bone marrow and circulating stem/progenitor cells for regenerative cardiovascular therapy.** Translational Research. 2010;156(3):112-29.
77. Leor J, Aboulafia-Etzion S, Dar A, Shapiro L, Barbash IM, Battler A, et al. **Bioengineered Cardiac Grafts : A New Approach to Repair the Infarcted Myocardium? Circulation.** 2000;102(Supplement 3): III-56-III-61.

78. Zimmermann W, Didie M, Doker S, Melnychenko I, Naito H, Rogge C, et al. **Heart muscle engineering: An update on cardiac muscle replacement therapy.** Cardiovascular Research. 2006;71(3):419-29.
79. Langer R, Vacanti J. **Tissue engineering.** Science. 1993;260(5110):920-6.
80. Masuda S, Shimizu T, Yamato M, Okano T. **Cell sheet engineering for heart tissue repair.** Advanced Drug Delivery Reviews. 2008;60(2):277-85.
81. Matsuda N, Shimizu T, Yamato M, Okano T. **Tissue Engineering Based on Cell Sheet Technology.** Advanced Materials. 2007;19(20):3089-99.
82. Birks EJ, Tansley PD, Hardy J, George RS, Bowles CT, Burke M, et al. ***Left Ventricular Assist Device and Drug Therapy for the Reversal of Heart Failure.*** New England Journal of Medicine. 2006;355(18):1873-84.
83. Laflamme MA, Murry CE. **Regenerating the heart.** Nature Biotechnology. 2005;23(7):845-56.
84. Chen Q-Z, Harding SE, Ali NN, Lyon AR, Boccaccini AR. **Biomaterials in cardiac tissue engineering: Ten years of research survey.** Materials Science and Engineering: R: Reports. 2008;59(1-6):1-37.

85. Giraud M-N, Armbruster C, Carrel T, Tevæarai HT. **Current State of the Art in Myocardial Tissue Engineering.** Tissue Engineering. 2007;13(8):1825-36.
86. Luque EA, Veenstra RD, Beyer EC, Lemanski LF. *Localization and distribution of gap junctions in normal and cardiomyopathic hamster heart.* Journal of Morphology. 1994;222(2):203-13.
87. Bennett MVL, Spray DC, Harris AL. **Electrical Coupling in Development.** American Zoologist. 1981;21(2):413-27.
88. Haraguchi Y, Shimizu T, Yamato M, Kikuchi A, Okano T. **Electrical coupling of cardiomyocyte sheets occurs rapidly via functional gap junction formation.** Biomaterials. 2006;27(27):4765-74.
89. Sun H, Lü S, Jiang X-X, Li X, Li H, Lin Q, et al. **Carbon nanotubes enhance intercalated disc assembly in cardiac myocytes via the β 1-integrin-mediated signaling pathway.** Biomaterials. 2015;55:84-95.
90. da Silva EE, Della Colleta HHM, Ferlauto AS, Moreira RL, Resende RR, Oliveira S, et al. **Nanostructured 3-D collagen/nanotube biocomposites for future bone regeneration scaffolds.** Nano Research. 2010;2(6):462-73.
91. Bianco A, Prato M. **Can Carbon Nanotubes be Considered Useful Tools for Biological Applications?** Advanced Materials. 2003;15(20):1765-8.

92. Lewitus DY, Landers J, Branch JR, Smith KL, Callegari G, Kohn J, et al. **Biohybrid Carbon Nanotube/Agarose Fibers for Neural Tissue Engineering.** *Advanced Functional Materials.* 2011;21(14):2624-32.
93. MacDonald RA, Voge CM, Kariolis M, Stegemann JP. **Carbon nanotubes increase the electrical conductivity of fibroblast-seeded collagen hydrogels.** *Acta Biomaterialia.* 2008;4(6):1583-92.
94. Vasita R, Katti DS. *Nanofibers and their applications in tissue engineering.* *International Journal of Nanomedicine.* 2006;1(1):15-30.
95. MacDonald RA, Laurenzi BF, Viswanathan G, Ajayan PM, Stegemann JP. *Collagen-carbon nanotube composite materials as scaffolds in tissue engineering.* *Journal of Biomedical Materials Research Part A.* 2005;74A(3):489-96.
96. Mikael PE, Amini AR, Basu J, Josefina Arellano-Jimenez M, Laurencin CT, Sanders MM, et al. **Functionalized carbon nanotube reinforced scaffolds for bone regenerative engineering: fabrication, in vitro and in vivo evaluation.** *Biomedical Materials.* 2014;9(3).
97. Lalwani G, Gopalan A, D'Agati M, Srinivas Sankaran J, Judex S, Qin Y-X, et al. *Porous three-dimensional carbon nanotube scaffolds for tissue engineering.* *Journal of Biomedical Materials Research Part A.* 2015;103(10):3212-25.

98. Shin SR, Zihlmann C, Akbari M, Assawes P, Cheung L, Zhang K, et al. **Reduced Graphene Oxide-GelMA Hybrid Hydrogels as Scaffolds for Cardiac Tissue Engineering.** *Small*. 2016;12(27):3677-89.
99. Sun H, Zhou J, Huang Z, Qu L, Lin N, Liang C, et al. ***Carbon nanotube-incorporated collagen hydrogels improve cell alignment and the performance of cardiac constructs.*** *International Journal of Nanomedicine*. 2017;Volume 12:3109-20.
100. Assali M, Kittana N, Qasem SA, Adas R, Saleh D, Arar A, et al. **Combretastatin A4-camptothecin micelles as combination therapy for effective anticancer activity.** *RSC Advances*. 2019;9(2):1055-61.
101. Alsouqi DG. **Functionalization of graphene sheets and their antibacterial activity.** Nablus, Palestine: An-Najah National University; 2017.
102. Hamad DF. **Bio-Functionalization of SWCNTs with Combretastatin A4 for Targeted Cancer Therapy.** Nablus-Palestine: An-Najah National University; 2017.
103. Shiraki I, Nagao T, Hasegawa S, Petersen CL, BØGgild P, Hansen TM, et al. **Micro-Four-Point Probes in a Uhv Scanning Electron Microscope for in-Situ Surface-Conductivity Measurements.** *Surface Review and Letters*. 2012;07(05n06):533-7.

104. Bowler N. **Four-point potential drop measurements for materials characterization.** Measurement Science and Technology. 2011;22(1).
105. Valdes L. **Resistivity Measurements on Germanium for Transistors.** Proceedings of the IRE. 1954;42(2):420-7.
106. Chan W-F, Chen H-y, Surapathi A, Taylor MG, Shao X, Marand E, et al. **Zwitterion Functionalized Carbon Nanotube/Polyamide Nanocomposite Membranes for Water Desalination.** ACS Nano. 2013;7(6):5308-19.
107. Assali M, Leal MP, Fernández I, Baati R, Mioskowski C, Khier N. **Non-covalent functionalization of carbon nanotubes with glycolipids: glyconanomaterials with specific lectin-affinity.** Soft Matter. 2009;5(5).
108. Kolb HC, Finn MG, Sharpless KB. **Click Chemistry: Diverse Chemical Function from a Few Good Reactions.** Angewandte Chemie International Edition. 2001;40(11):2004-21.
109. Wang K, Guo Z, Zhang L, Sun K, Yu P, Zhou S, et al. **Co-assembly of donor and acceptor towards organogels tuned by charge transfer interaction strength.** Soft Matter. 2017;13(10):1948-55.
110. Sun Y-P, Fu K, Lin Y, Huang W. **Functionalized Carbon Nanotubes: Properties and Applications.** Accounts of Chemical Research. 2002;35(12):1096-104.

111. Ghaemi F, Abdullah LC, Kargarzadeh H, Abdi MM, Azli NFWM, Abbasian M. **Comparative Study of the Electrochemical, Biomedical, and Thermal Properties of Natural and Synthetic Nanomaterials.** *Nanoscale Research Letters*. 2018;13(1).
112. Bhattacharjee S. *DLS and zeta potential – What they are and what they are not?* **Journal of Controlled Release**. 2016;235:337-51.
113. Kittana N, Assali M, Abu-Rass H, Lutz S, Hindawi R, Ghannam L, et al. *Enhancement of wound healing by single-wall/multi-wall carbon nanotubes complexed with chitosan.* **International Journal of Nanomedicine**. 2018;Volume 13:7195-206.

جامعة النجاح الوطنية

كلية الدراسات العليا

التفعيل غير التناسقي للمواد النانوية الكربونية باعتبارها هيكل بنائي

لهندسة الأنسجة

إعداد

سحر إياد عبد الرحمن الحاج قاسم

إشراف

د. محي الدين العسالي

د. نعيم كتانة

قدمت هذه الأطروحة استكمالاً لمتطلبات الحصول على درجة الماجستير في العلوم الصيدلانية،
بكلية الدراسات العليا، في جامعة النجاح الوطنية، نابلس - فلسطين.

2020

ب

التفعيل غير التناسقي للمواد النانوية الكربونية باعتبارها هيكل بنائي لهندسة الأنسجة

إعداد

سحر إياد عبد الرحمن الحاج قاسم

إشراف

د. محي الدين العسالي

د. نعيم كتانة

الملخص

هندسة الأنسجة هي أحد الموضوعات المثيرة في البحث الحديث والذي يحتاج إلى متطلبات خاصة تعتمد على السقالة المطورة لتحقيق نمو ناجح للنسيج. تم تحقيق تقدم متنوع لتطوير المواد الحيوية المناسبة التي توفر سقالة جيدة مع المسامية المثلى، والخصائص الميكانيكية والكهربائية. في السنوات الأخيرة، تم إيعاز اهتمام كبير للمواد النانوية الكربونية ومواد الكولاجين المركبة وتطبيقاتها في مجال هندسة الأنسجة.

ومع ذلك، تعاني المواد النانوية الكربونية من انخفاض قابلية الذوبان في الماء مما يعرقل استخدامها. لذلك، نهدف إلى التفعيل غير تساهمي للمواد النانوية الكربونية مع جزء البيرين واستخدام رابط مائي مناسب -مشتق من البولي إيثيلين جليكول- لتذويب الهياكل النانوية الكربونية في الماء. ستحافظ هذه الرابطة غير التساهمية على الخصائص الإلكترونية للبنية النانوية الكربونية لتكون سقالة مناسبة لهندسة الأنسجة. تم توصيف هذه المواد النانوية الكربونية المفعلة بالميكروسكوب الإلكتروني النافذ. أظهرت صور الميكروسكوب الإلكتروني النافذ تشيئًا جيدًا للمواد النانوية الكربونية المفعلة بقطر يتراوح من (5-15) نانومتر لأنابيب الكربون النانوبه و(0.6-0.8) ميكرومتر لصفائح الجرافين المفعلة. أيضا، تم تأكيد ترابط بي-بي الناجح بين مشتقات البيرين والبنية النانوية الكربونية بواسطة أطياف الامتصاص. علاوة على ذلك، تم استخدام التحليل الحراري الوزني لتحديد كمية المواد النانوية الكربونية المفعلة والتي تتراوح في نطاق

(17-29)%. وأخيراً، تم استخدام تحليل جهد الزيتا وتم الحصول في جميع الحالات على قيم تتراوح حول 20- ملفولت والتي تشير إلى تكوين محاليل معلق مستقره.

تم إنشاء الانسجة الضامة المهندسة (ECTs) والقائمة على خلايا 3T3 بتركيز مختلفة من المواد النانوية الكربونية. الانسجة المطورة اظهرت تحسن كبير في الموصلية الكهربائية وبالتالي الموصلية تعتمد في الغالب على النوع المستخدم. بينما في ECTs التي تحتوي على الخلايا الليفية الجلدية الأولية أظهرت موصلية اقل للكهرباء. تم تأكيد حيوية خلايا 3T3 باستخدام فحص ال MTS وأظهرت البيانات أن التراكيز 0.025% من الأنابيب النانوية الكربونية و0.005% من مشتقات الجرافين قللت من قدرة الخلية على البقاء بين حوالي (10-30) %. تم ايجاد ان هذه التراكيز كافية لتعزيز الموصلية الكهربائية للأنسجة بشكل ملحوظ. جميع الانسجة المفحوصة قد قللت بشكل ملحوظ من درجة تليف الأنسجة بالمقارنة مع الأنسجة الخالية من مواد الكربون النانويه باستثناء تركيز 0.020% من graphene-Py-COOH الذي أظهر درجة من التليف مماثلة للنسيج الضابط. سمك ألياف الكولاجين في جميع الظروف المستخدمة كان مشابه لتلك الخاصة بالنسيج الضابط باستثناء تركيز 0.005% من ال graphene-Py-COOH الذي أظهر انخفاضاً ملحوظاً. بالاضافه الى ذلك أظهرت جميع الانسجة المطورة انخفاضاً ملحوظاً في مسامية المصفوفة بالمقارنة مع النسيج الضابط. بينما في ECTs التي تحتوي على الخلايا الليفية الجلدية الأولية لم تظهر جميع ال ECTs من الأنابيب النانوية الكربونية وحمولات الجرافين أي تغيير ذي دلالة إحصائية على سمك ألياف الكولاجين بالمقارنة مع النسيج الضابط. من خلال أخذ هذا مع بيانات الموصلية يمكن افتراض أن مسامية ال ECT وموصلية النسيج لا يوجد ترابط بينهم.

